

Supplementary Information for Barometers Behaving Badly

Penny E. Wieser^{1*},², Adam Kent², Christy B. Till³, John Donovan⁴, David A. Neave⁵, Dawnika Blatter⁶, Michael J. Krawczynski⁷

1. Corresponding author: Penny_wieser@berkeley.edu, 541–908–4572. Department of Earth and Planetary Sciences, McCone Hall, UC Berkeley, 94720, USA

2. College of Earth, Ocean and Atmospheric Sciences, Oregon State University, 97331, USA

3. School of Earth and Space Exploration, Arizona State University, Tempe, AZ 85281, USA

4. Department of Earth Sciences, University of Oregon, 97403, USA.

5. Department of Earth and Environmental Sciences, The University of Manchester, Oxford Road, Manchester M13 9PL, UK

6. U.S. Geological Survey, Volcano Science Center, 345 Middlefeld Road, Menlo Park, CA 94025, USA

7. Department of Earth and Planetary Sciences, Washington University in St. Louis, 1 Brookings Drive, St. Louis, MO 63130, USA

1. Compilation of beam currents and count times used for Na

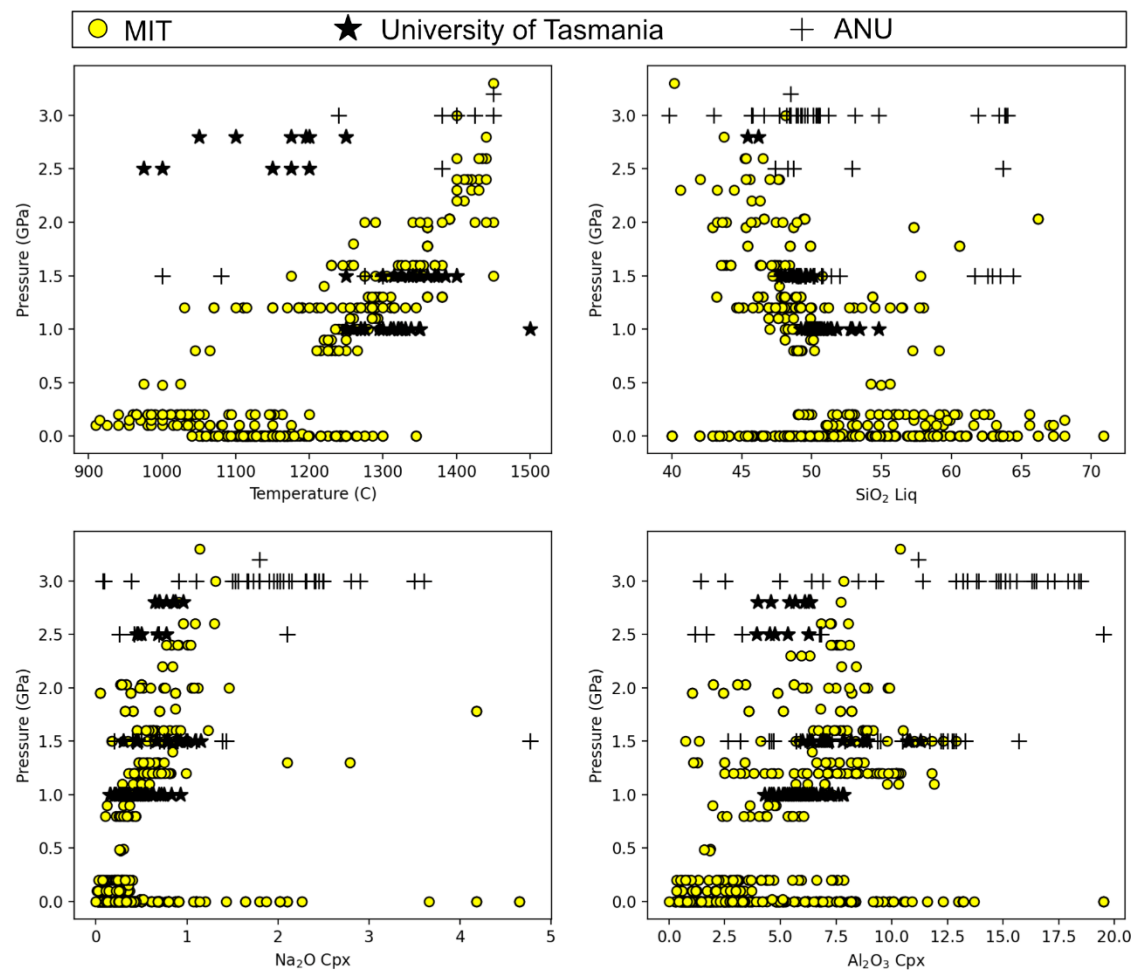
Supporting Table 1- *Compilation of beam current and count times for Na analyses in a subset of the LEPF dataset conducted at <1 GPa used to calibrate most existing thermobarometers. Missing or incomplete/ambiguous data are colored orange.*

Reference	Beam Current (I)	Count time (t)	I*t	Instrument
Akella (1976)				
Baker and Eggler (1987)	12 nA			Penn State + Smithsonian
Gee and Sack (1988)	30 nA	2-10 s	60-300	JEOL Superprobe Northwestern, ARL UC Berkeley
Carroll and Wyllie (1989)	5 nA			JEOL at Caltech, Cameca at Brown
Kennedy et al. (1990)	10 nA			MIT MAC-5 and JEOL 733

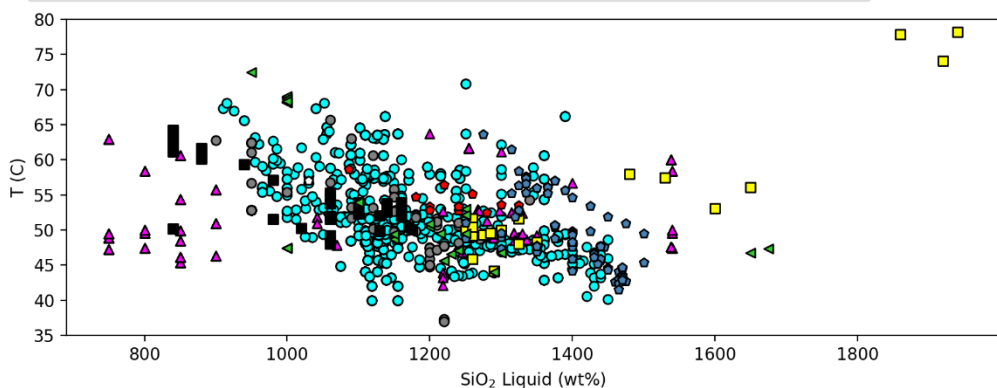
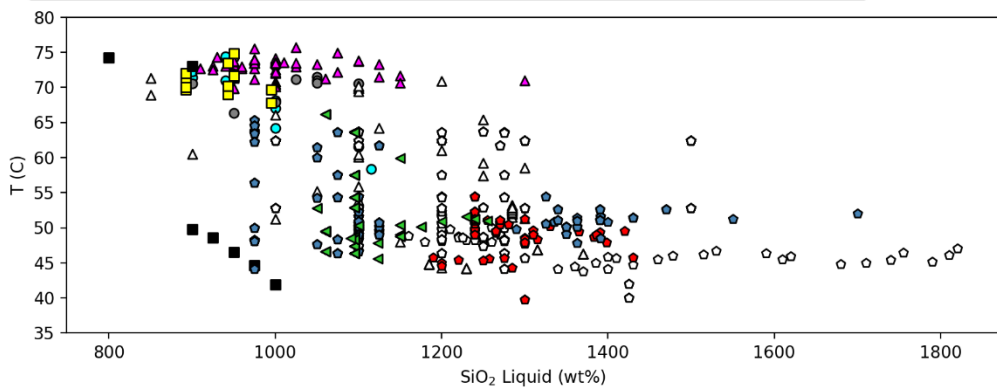
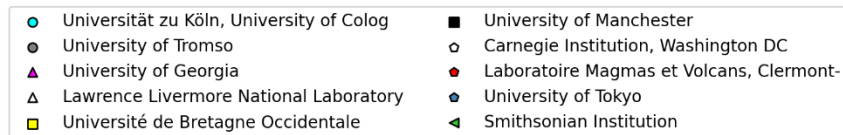
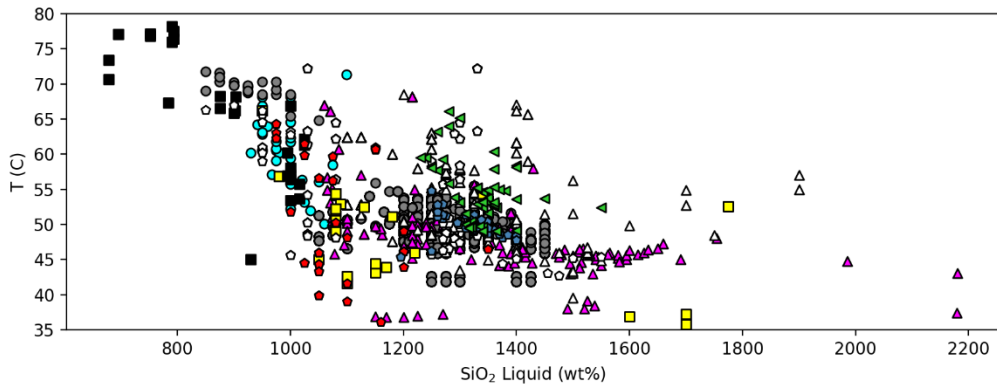
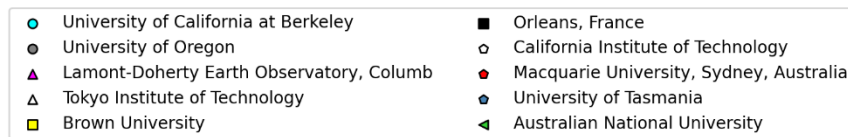
Nielsen et al. (1992)	20 nA	10 s	200	SX50, OSU
Fram and Longhi (1992)	5 nA			
Rushmer (1993)				SX50 (no loc, authors at ETH)
Baker et al. (1994)	10 nA			JEOL 733, Caltech
Baker et al. (1994)				MIT MAC-5 and JEOL 733
Draper and Johnston (1992)	20 nA	10 s	200	Cameca SX50, UOregon
Kawamoto (1996)				JEOL JSM-840 e, University of Tokyo
Springer and Seck (1997)	10 nA	5 s	50	camebax
Tsuruta and Takahashi (1998)	12 nA	10-40 s (don't specify for each element)	120-480	JEOL-JXA8800, Tokyo institute of technology
Métrich and Rutherford (1998)	15 nA			Camebax, Brown
Blundy et al. (1998)	15 nA			JEOL 833, University of Bristol
Draper and Green (1999)	20 nA	15 s	300 s	SX50, Macquarie
McCoy and Lofgren (1999)				JEOL JXA-8900R, Smithsonian
Wang and Takahashi (1999)	No information whatsoever on how phase compositions were measured (not even analytical technique)			
Minniti and Rutherford (2000)	15 nA			
Tielpo et al. (2000)				JEOL JXA-840A, Pavia
Blatter and Carmichael (2001)	20 nA			SX50, UC Berkeley
Wood and Trigila (2001)	15 nA	10-60 (don't say which element is which)	150 - 900	JEOL 8600, Bristol
Berndt et al. (2001)	18 nA	5 s	90	Camebax,
Toplis and Corgne (2002)	10 nA	Says 10s major 30s minor elements (no list)	300	Cameca SX50, Nancy
Scaillet (2003)	6 nA	10 s	60	(authors at Orleans)
Pertermann (2003)	7.5-15 nA	30 s	225-450	JXA8900R, Minnesota
Prouteau (2003)	6 nA	10 s	60	SX50, Orleans
Wasylewski (2003)	30 nA			Caltech JEOL733
Laporte et al. (2004)	15 nA	10s	150	SX-100, authors at Clermont-Ferrand
Maaløe (2004)	Uses EDS – no further information about analytical conditions. E.g. unclear if any standards used.			JEOL-2400 SEM
Barclay (2004)	20 nA	10 s	200	SX50, UC Berkeley
Feig et al. (2006)	15 nA	5 s	75	SX100,
Di Carlo (2006)	6 nA	10 s	60	SX-50, Orleans

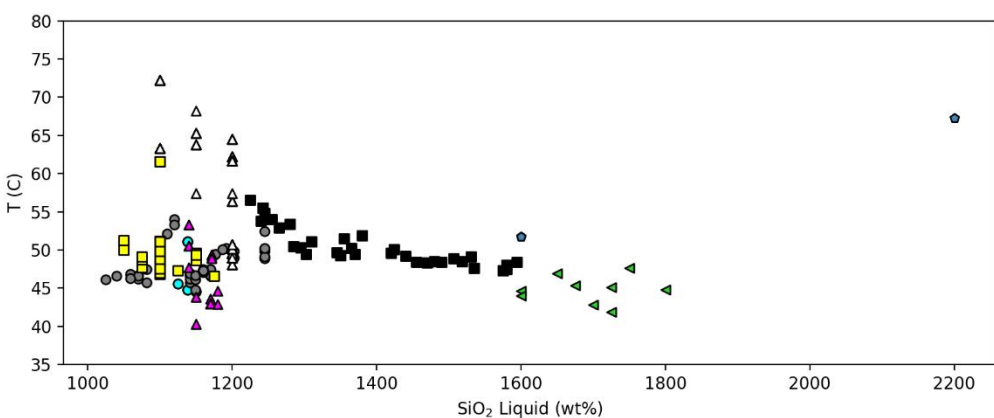
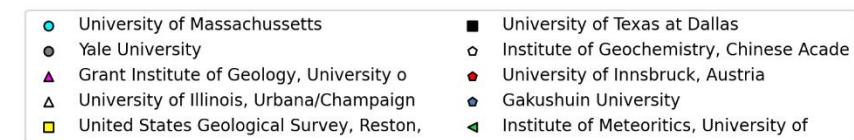
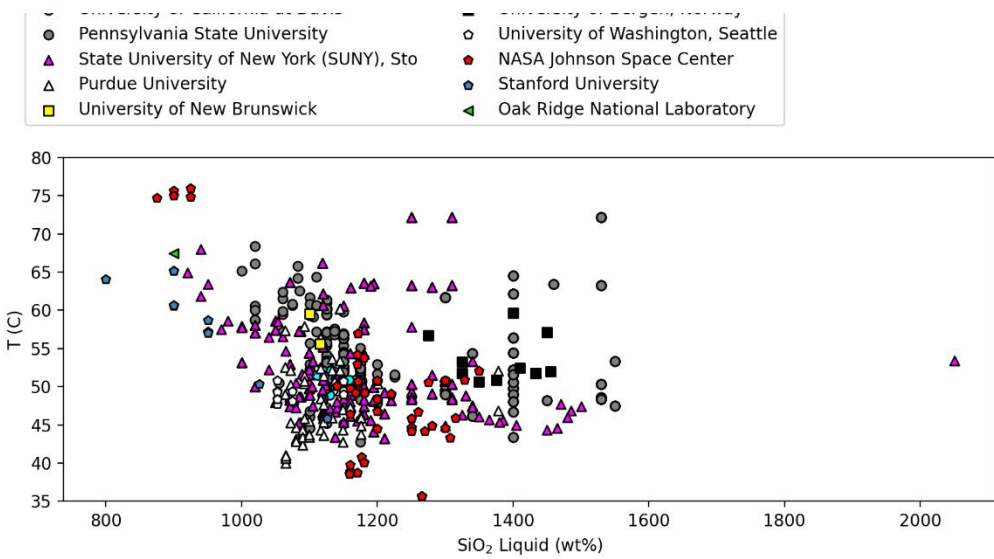
Scoates et al. (2006)	10 nA	10 s	100	Cameca SX-50, Université de Pierre
Alonso-Perez et al. (2009)	20 nA			SX50/JEOL 8600
Pertermann and Lundstrom (2006)	Use EDS on JEOL JSM 840 SEM with natural and synthetic standards. Some repeat analyses on JXA 8900, no mention of analytical conditions.			
new compilation				
Costa (2004)	12 nA	10 s	120	SX50 Orleans
Berndt (2004)	15 nA	5 s	75	SX100 Hannover
Pichavant and Macdonald (2007)	6 nA	6- 10 s	36-60	2 different Cameca, Orleans
Hamada and Fujii (2008)	12 nA			JEOL JXA8800R,
Feig et al. (2010)	15 nA	5 s	75	SX100, nd
Krawczynski et al. (2012)	10 nA	15 s	150	JEOL
Mandler et al. (2014)				JEOL JXA8200 Superprobe
Rader and Larsen (2013)	10 nA			Cameca SX-50, University of Alaska
Blatter et al. (2013)	15 nA	20 s	300	JEOL JXA-8900 Menlo Park
Almeev et al. (2013)	15 nA	8 s	120	SX100 Hannover
Cadoux et al. (2014)	6 nA	10 s	60	SX50 Orleans
Parat et al. (2014)	10 nA	10 s	100	SX100 montpellier
Melekhova et al. (2015)	No info for mineral analyses			SX100 Bristol
Andújar et al. (2015)	6 nA	10 s	60	SX50 Orleans
Nandedkar et al. (2014)	20 nA	20 s	400	JEOL JXA8200, nd, ETH?
Erdmann et al. (2016)	10 nA	10-20 s	100-200	
Husen et al. (2016)	10 nA	10 s	100	SX100 Hannover
Koepke et al. (2018)	15 nA	5 s	75	SX100,
Ulmer et al. (2018)	20 nA	20-30 s	400-600	ARL SEMQ/ SX50/JEOL JXA8200.
Neave et al. (2019)	10 nA	10 s	100	SX100 Hannover
Firth et al. (2019)	10 nA			SX100 Anu, Canberra, Macquarie
Waters et al. (2021)	10 nA	20 s	200	JEOL 8900 Superprobe, NHM

2. Further investigation of interlaboratory offsets

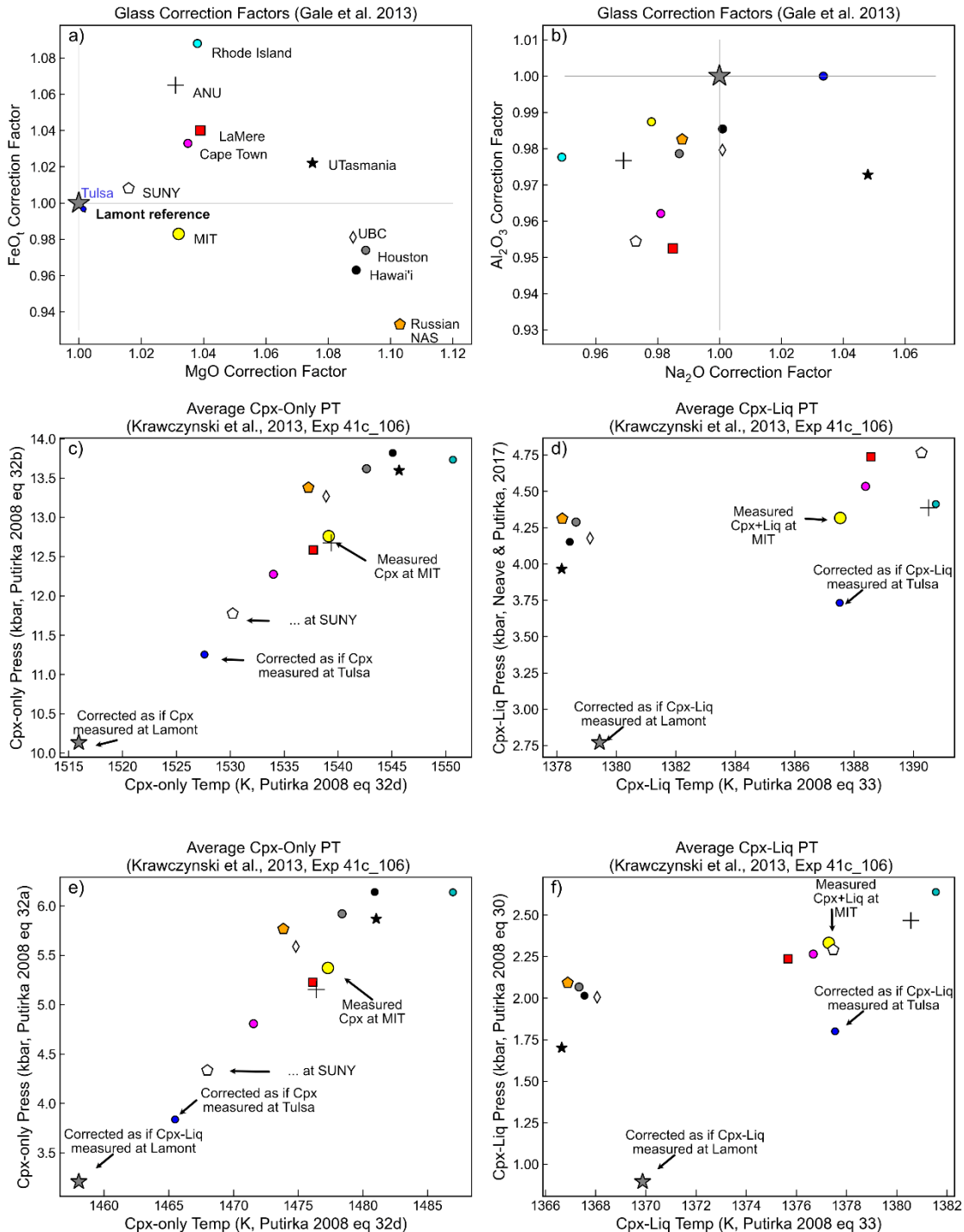


Supplementary Fig. 1 – Non-uniform distribution of P-T-X space covered by different laboratories.

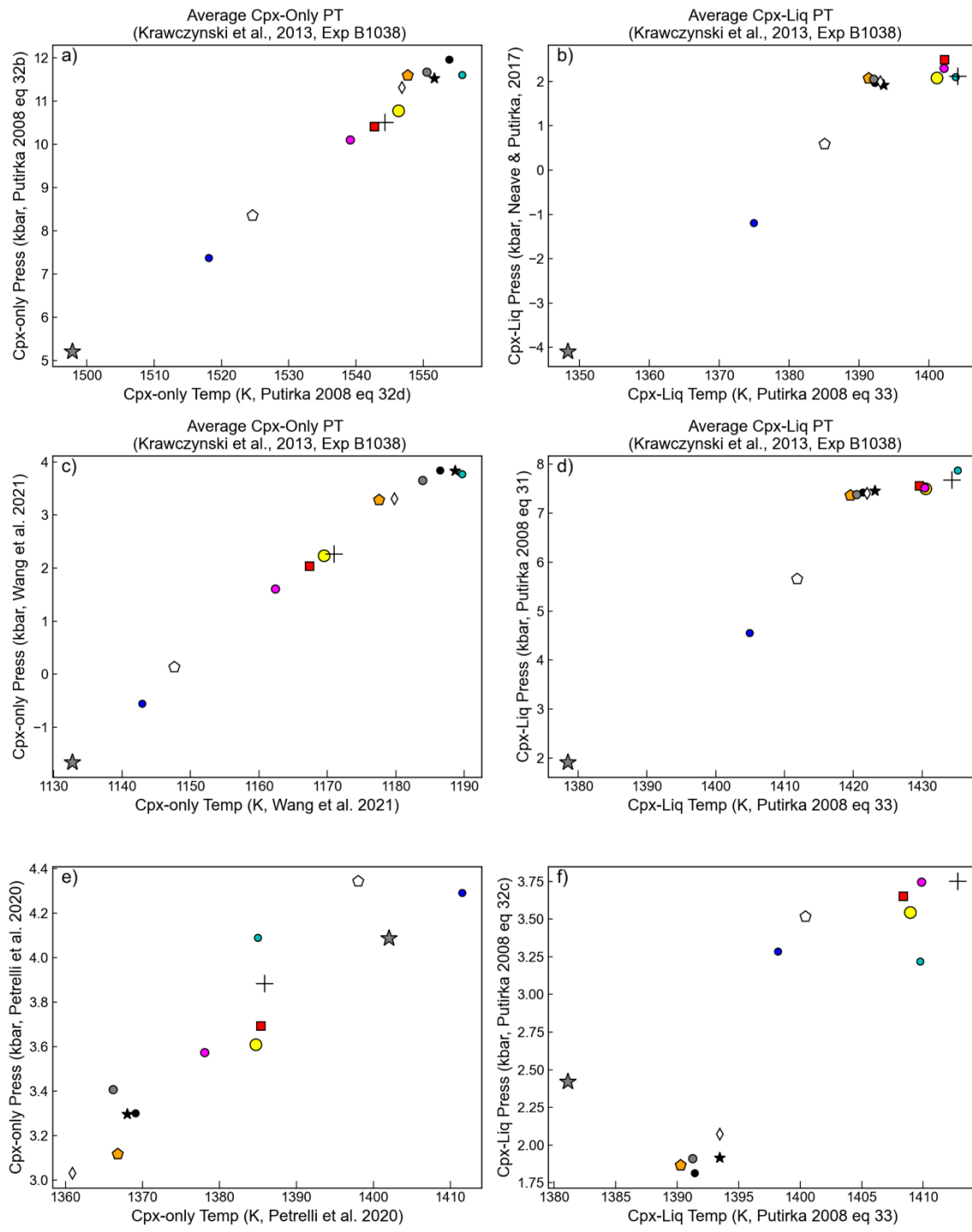




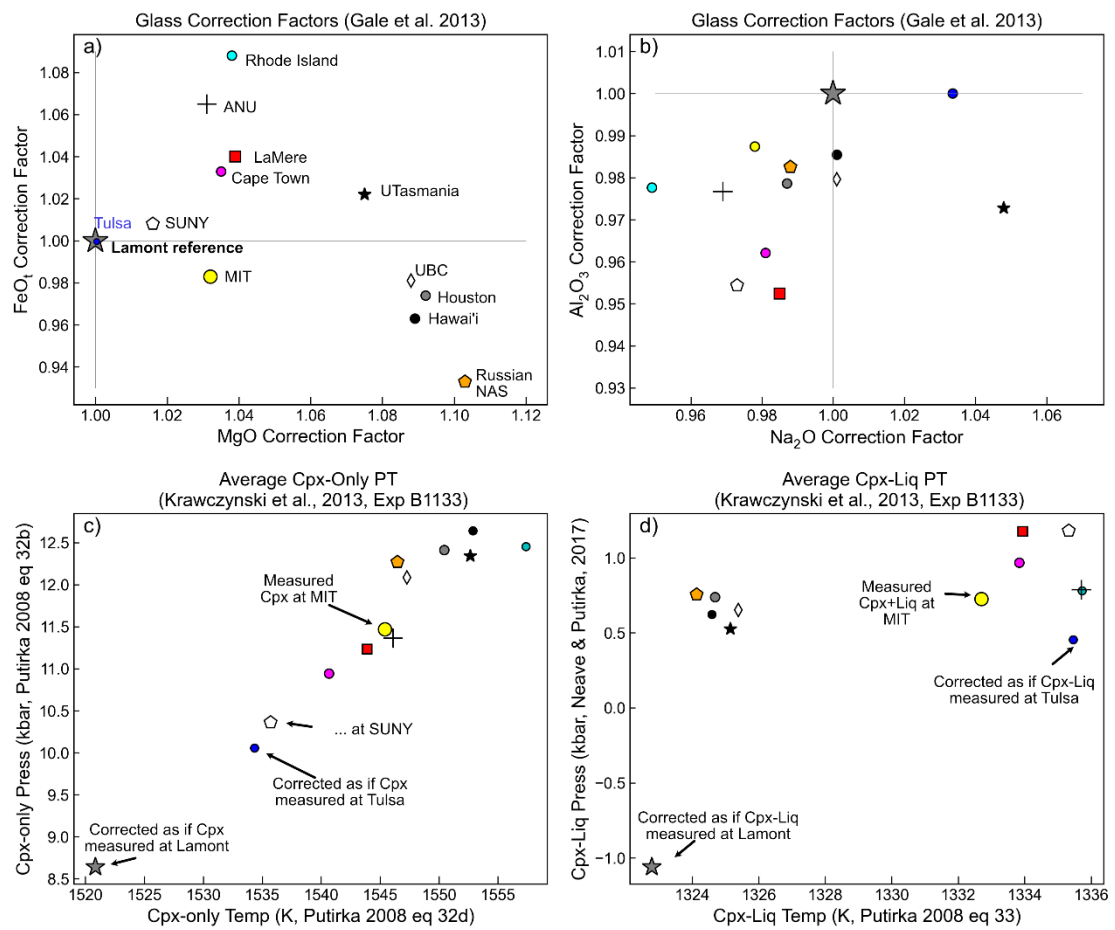
Supplementary Fig. 2 – Range of SiO_2 - T space covered by 47 different laboratories in the LEPR dataset.



Supporting Fig. 3 – First 4 panels as in main text, panel e-d showing the differences using eq32a for Cpx-only pressures (e) and equation 30 for Cpx-Liq pressures (d).

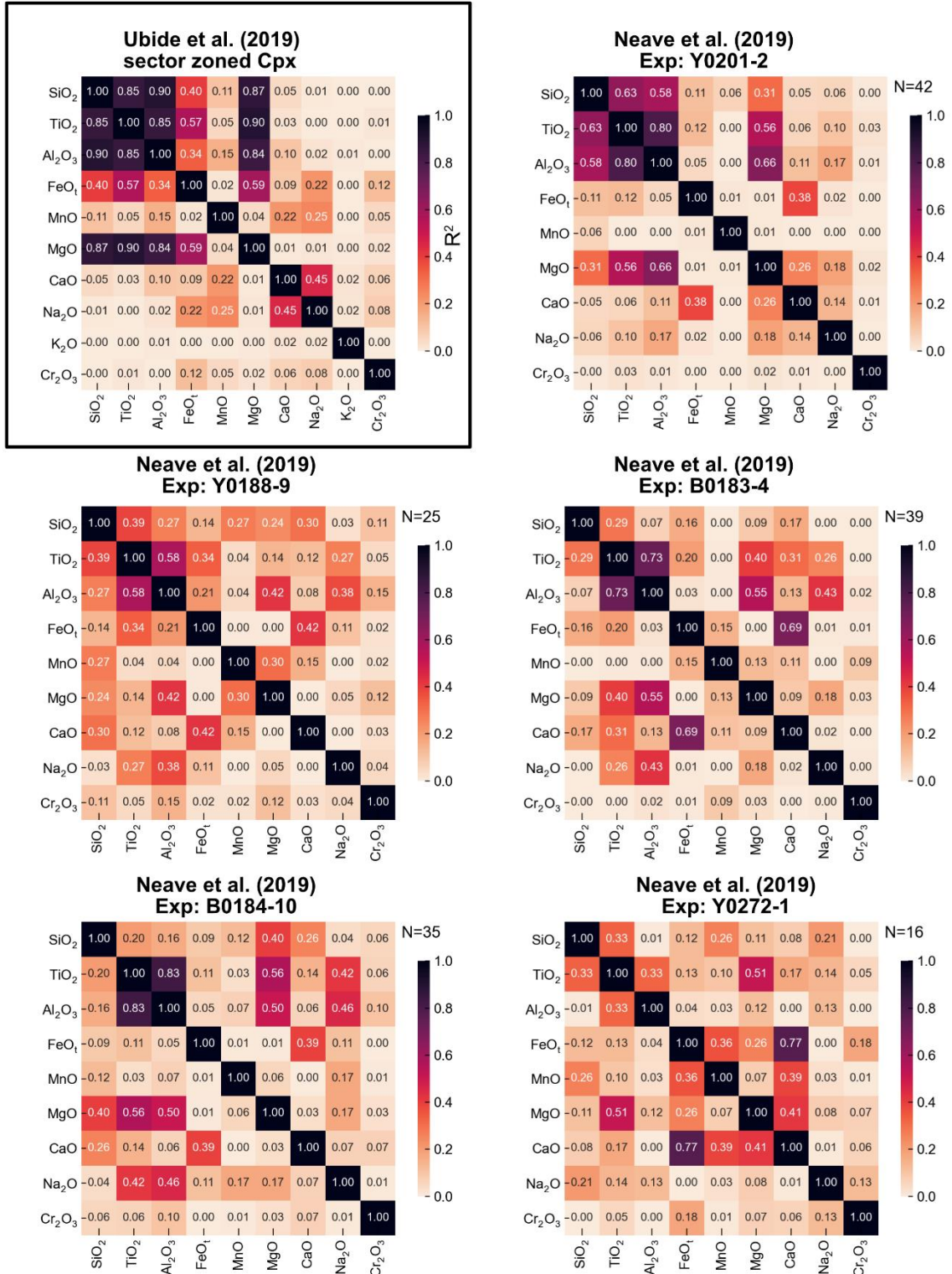


Supporting Fig. 4 – Using the same experiment as the bottom two panels in Fig. 2 of the main text for B1038 but showing discrepancies using different sets of barometers.

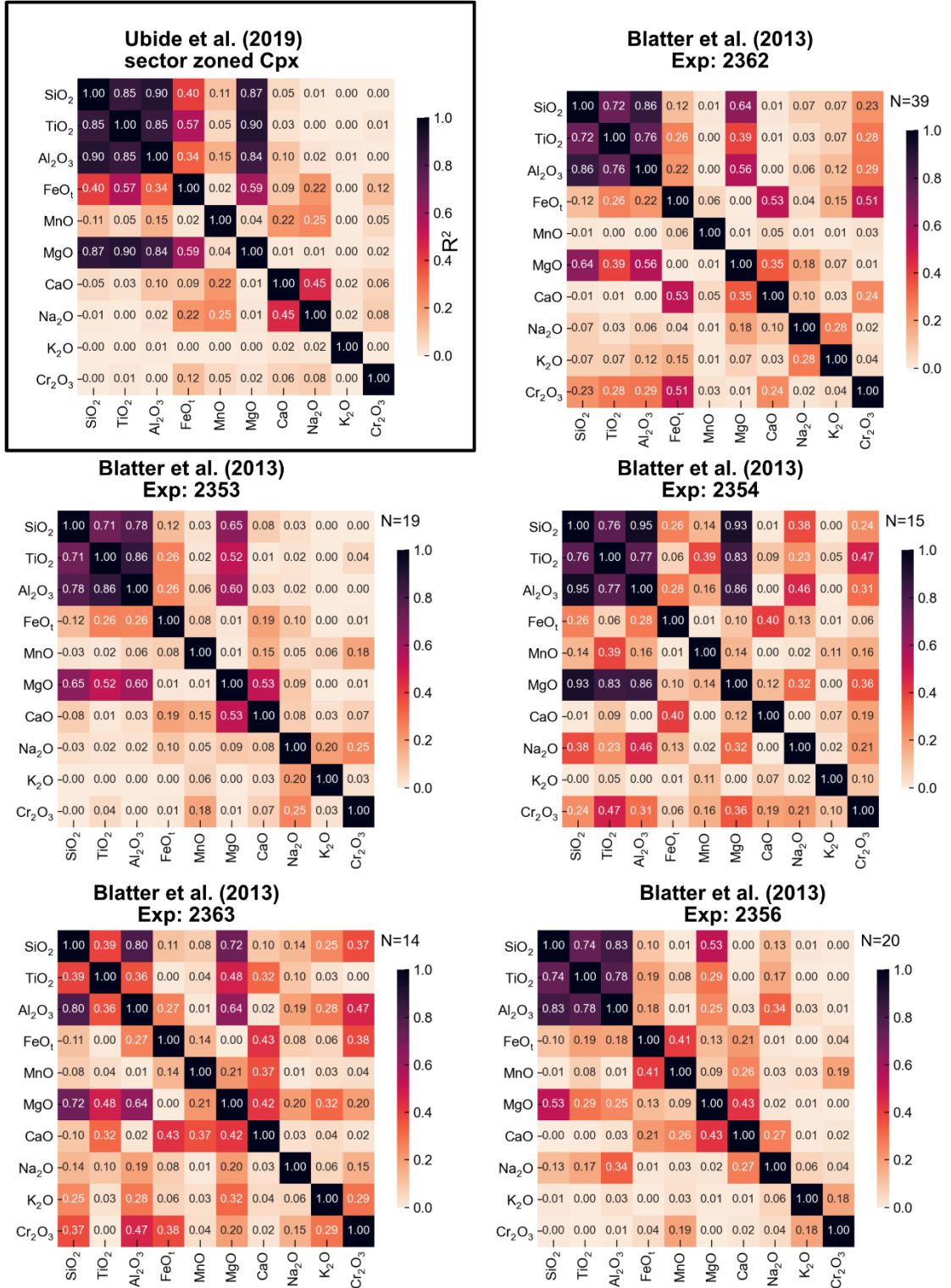


Supporting Fig. 5 – As for Fig. 2 of the main text but showing offsets for Experiment B1133.

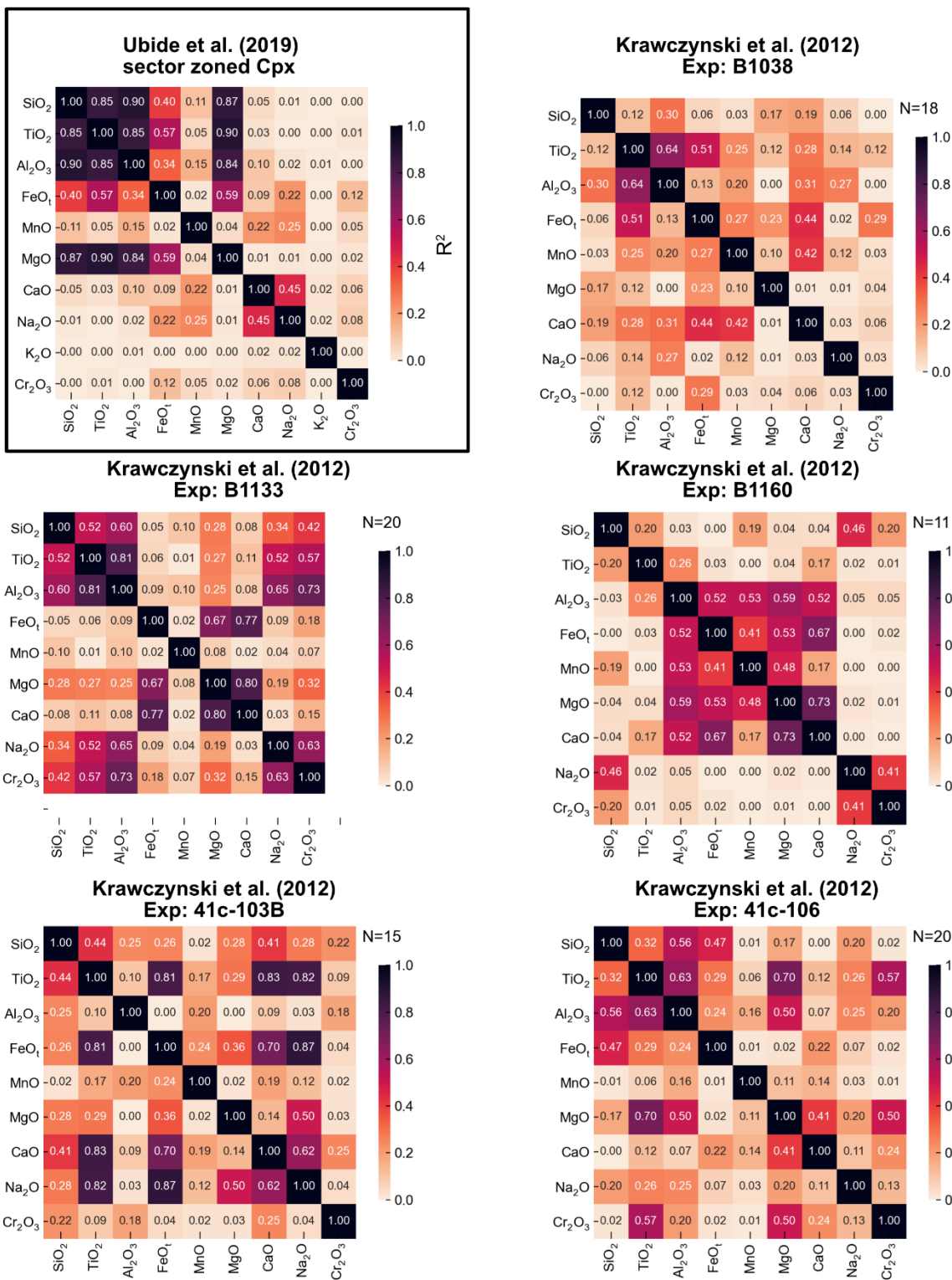
3. Covariance in Experimental Cpx Compositions



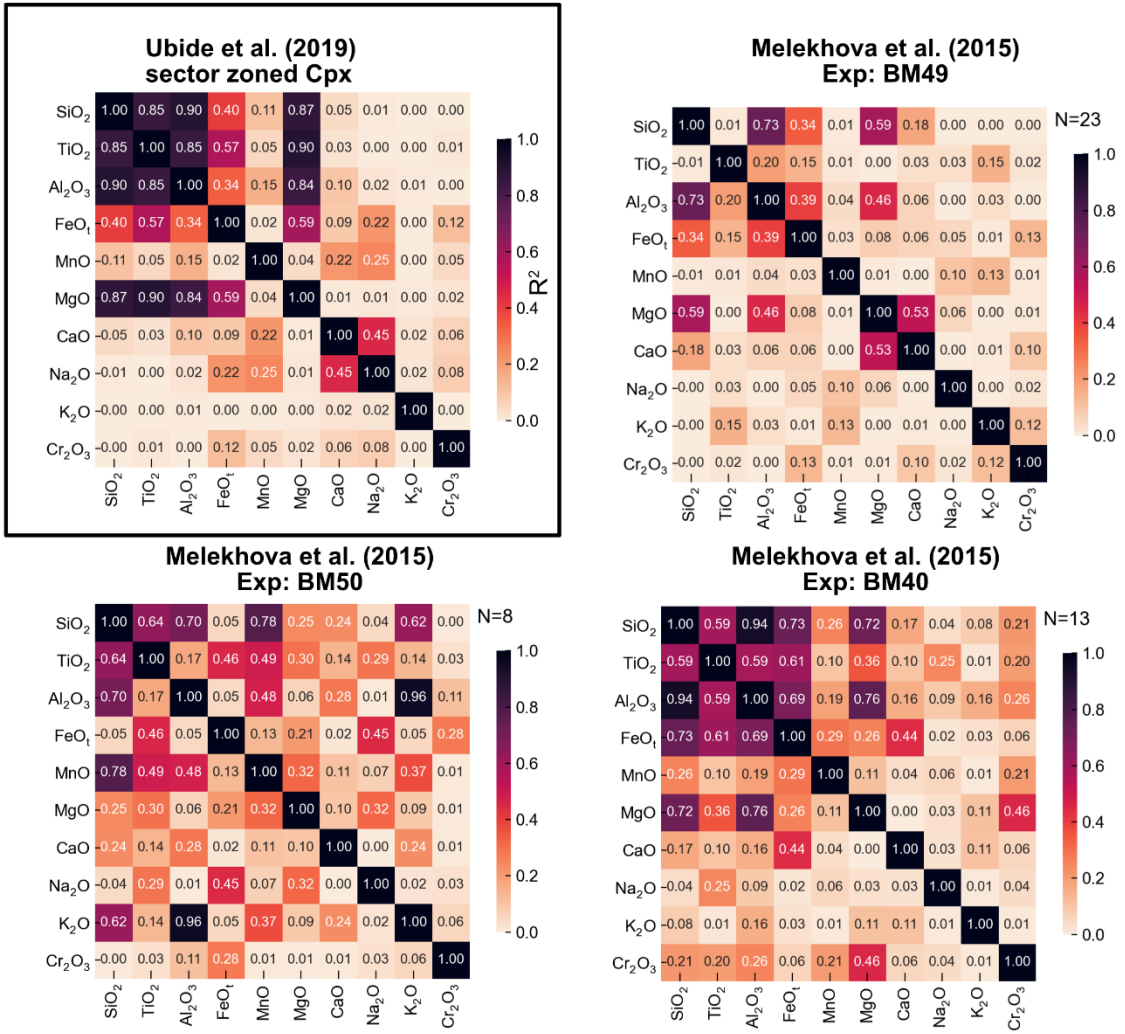
Supporting Fig. 6. Correlation matrix of pyroxenes from different experiments of Neave et al. (2019) with the color bar showing the R^2 value. The correlation matrix for the sector-zoned Cpx of Ubide et al. (2019) are shown for reference.



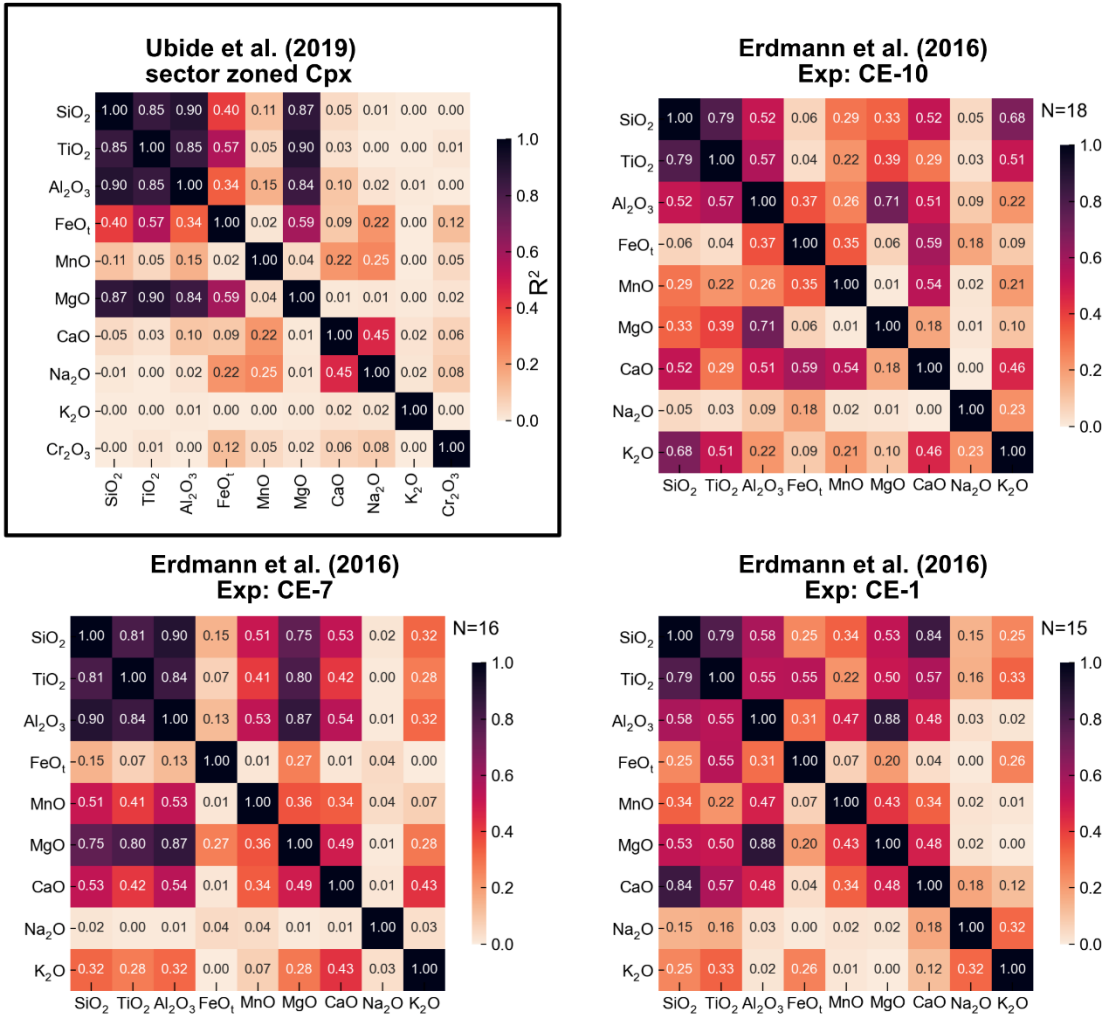
Supporting Fig 7 - Correlation matrix of pyroxenes from different experiments of Blatter et al. (2013) with the color bar showing the R^2 value. The correlation matrix for the sector-zoned Cpx of Ubide et al. (2019) are shown for reference.



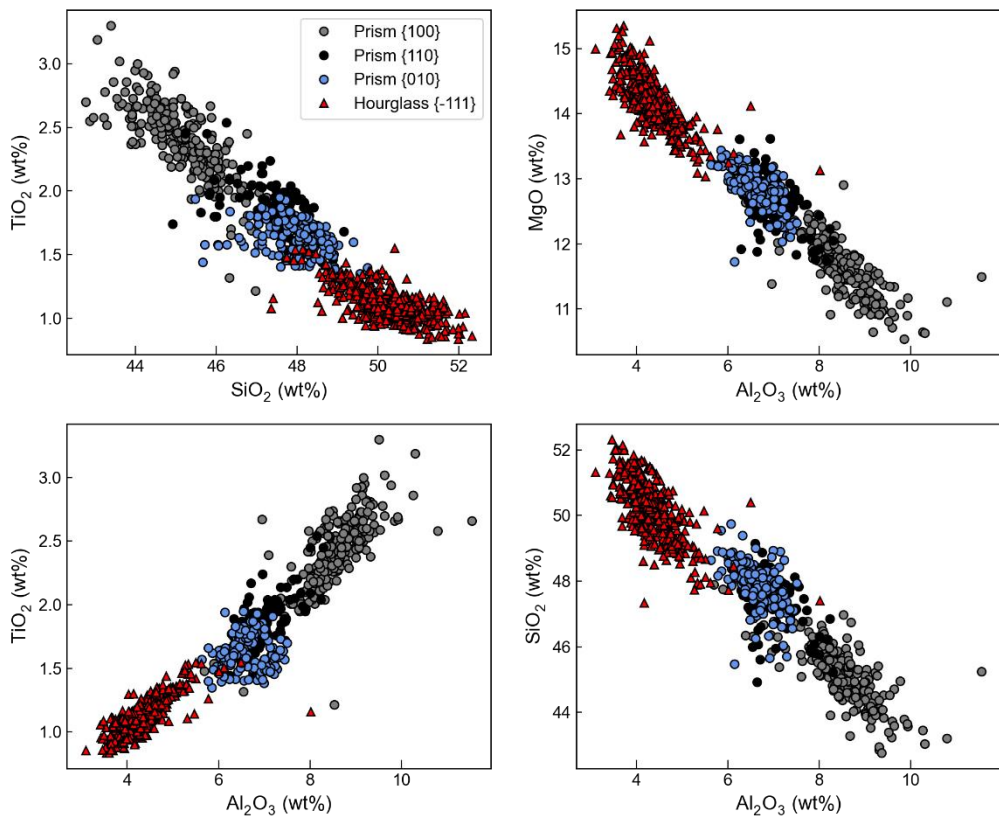
Supporting Fig 8 - Correlation matrix of pyroxenes from different experiments of Krawczynski et al. (2012) with the color bar showing the R² value. The correlation matrix for the sector-zoned Cpx of Ubide et al. (2019) are shown for reference.



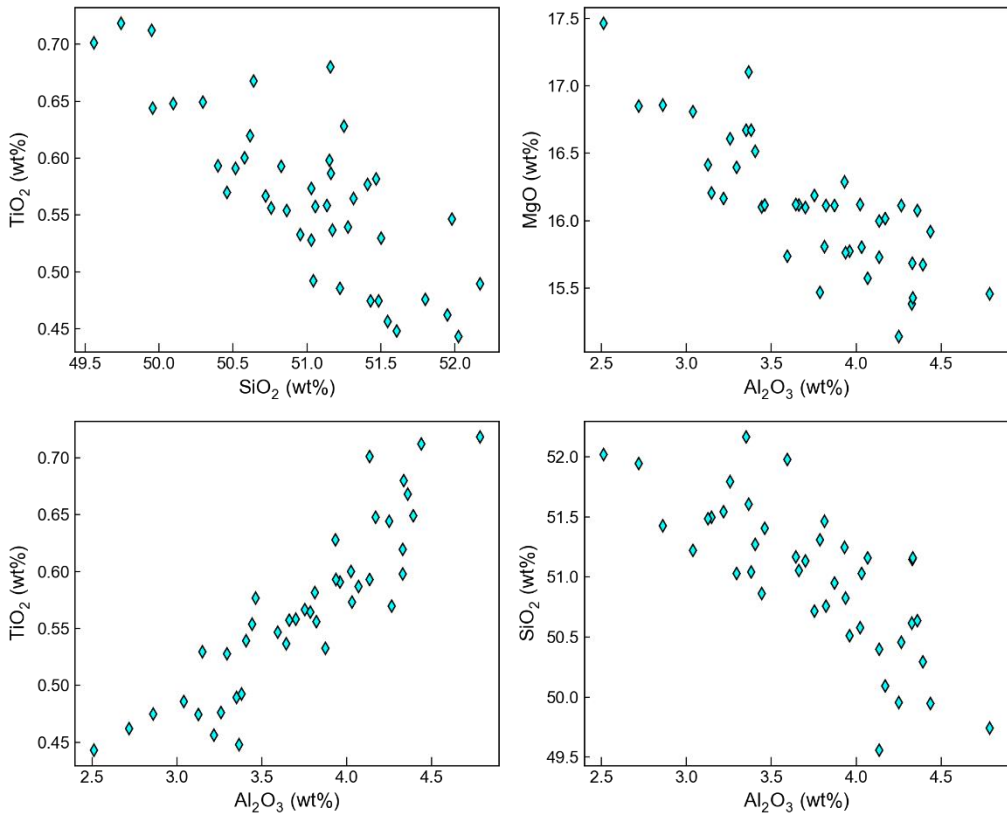
Supporting Fig 9 - Correlation matrix of pyroxenes from different experiments of Melekhova et al. (2015) with the color bar showing the R^2 value. The correlation matrix for the sector-zoned Cpx of Ubide et al. (2019) are shown for reference.



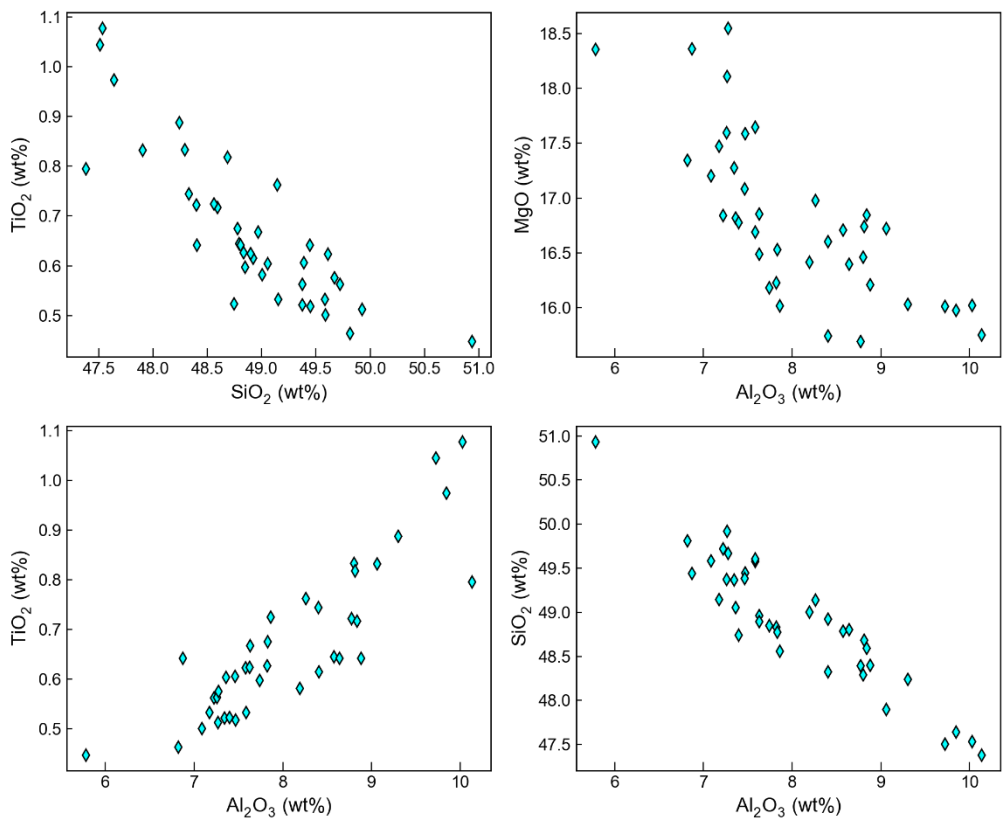
Supporting Fig 10 - Correlation matrix of pyroxenes from different experiments of Erdmann et al. (2016) with the color bar showing the R^2 value. The correlation matrix for the sector-zoned Cpx of Ubide et al. (2019) are shown for reference.



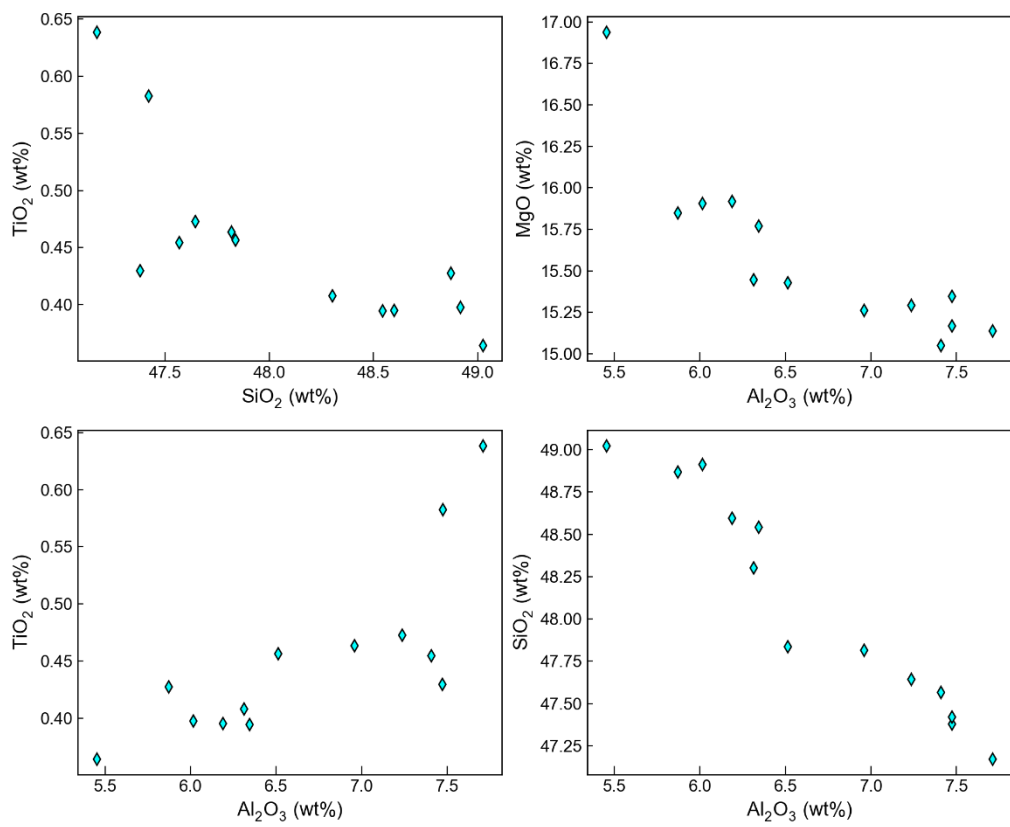
Supporting Fig. 11 : Major element correlations in sector zoned pyroxenes from Ubide et al. (2019), colored by sector.



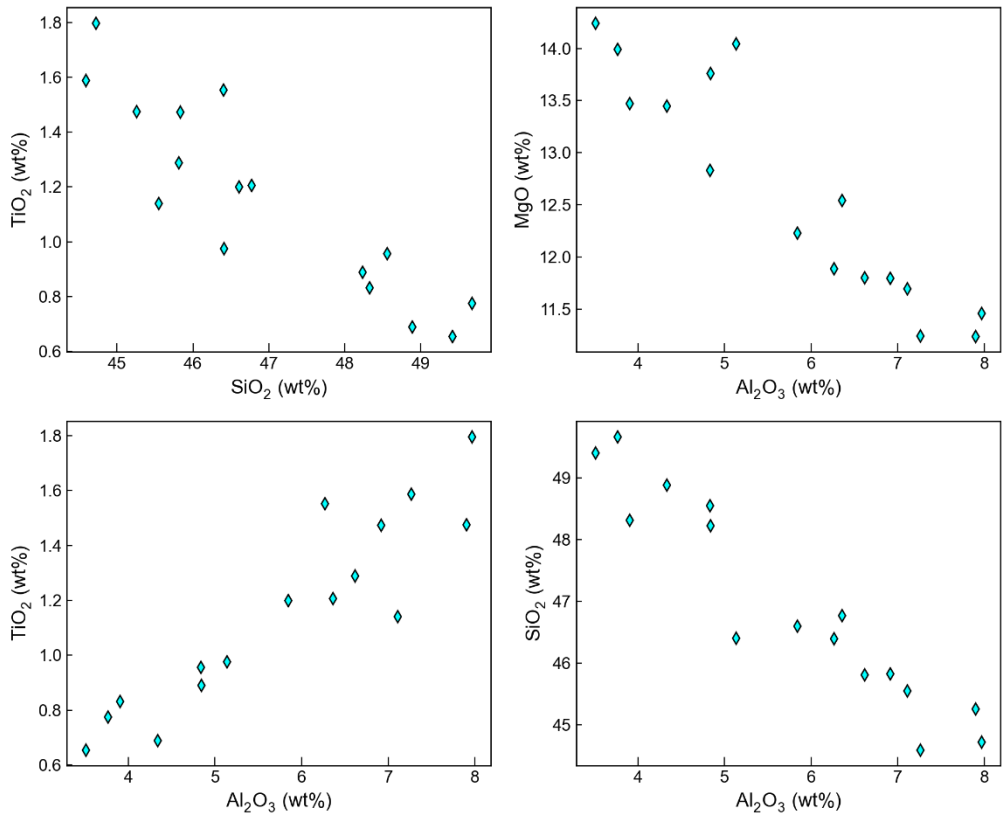
Supporting Figure 12 – Correlations between elements in Exp. Y0201-2 from Neave et al. (2017).



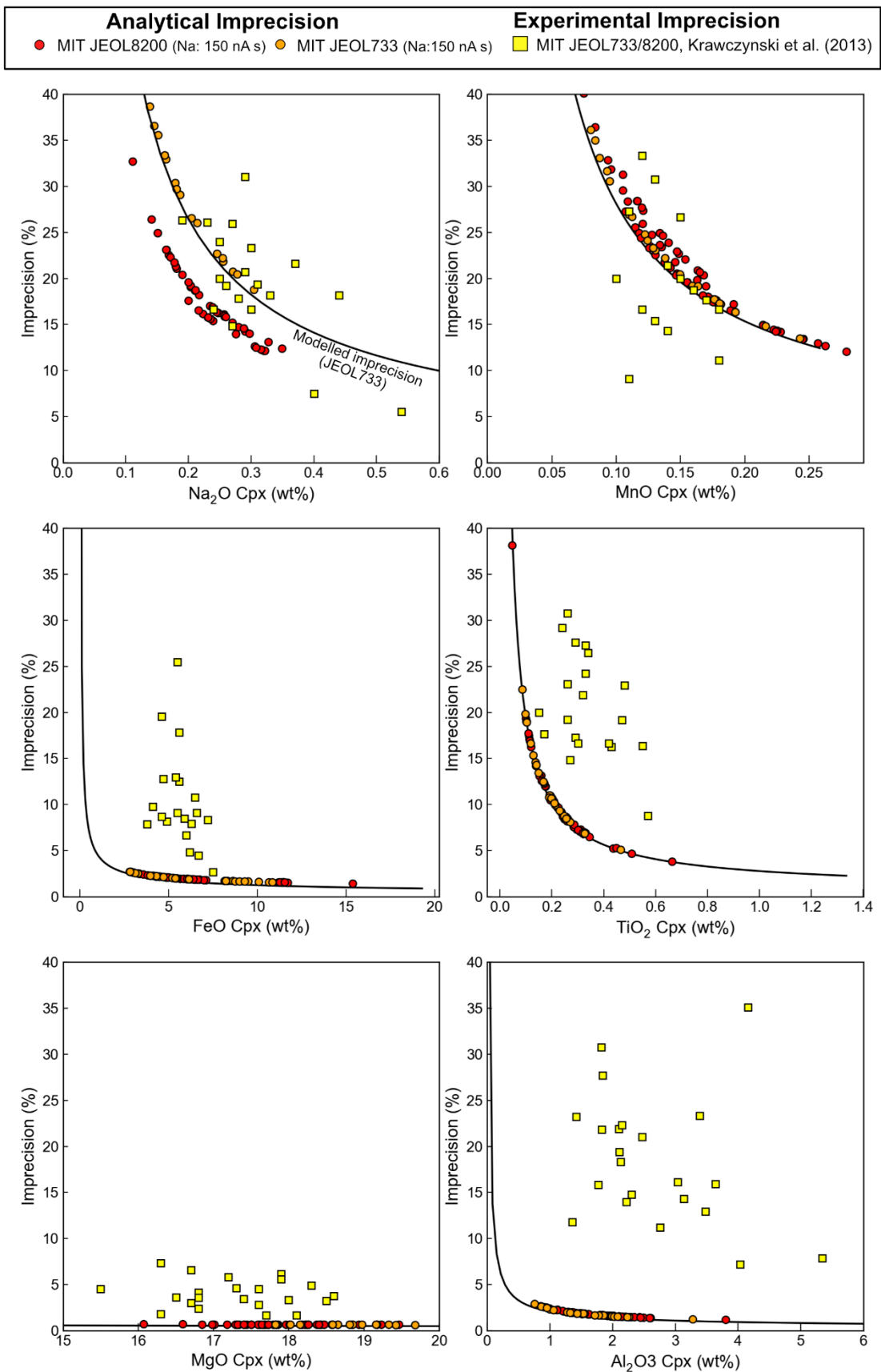
Supporting Figure 13 – Correlations between elements in Exp. 2362 from Blatter et al. (2013)



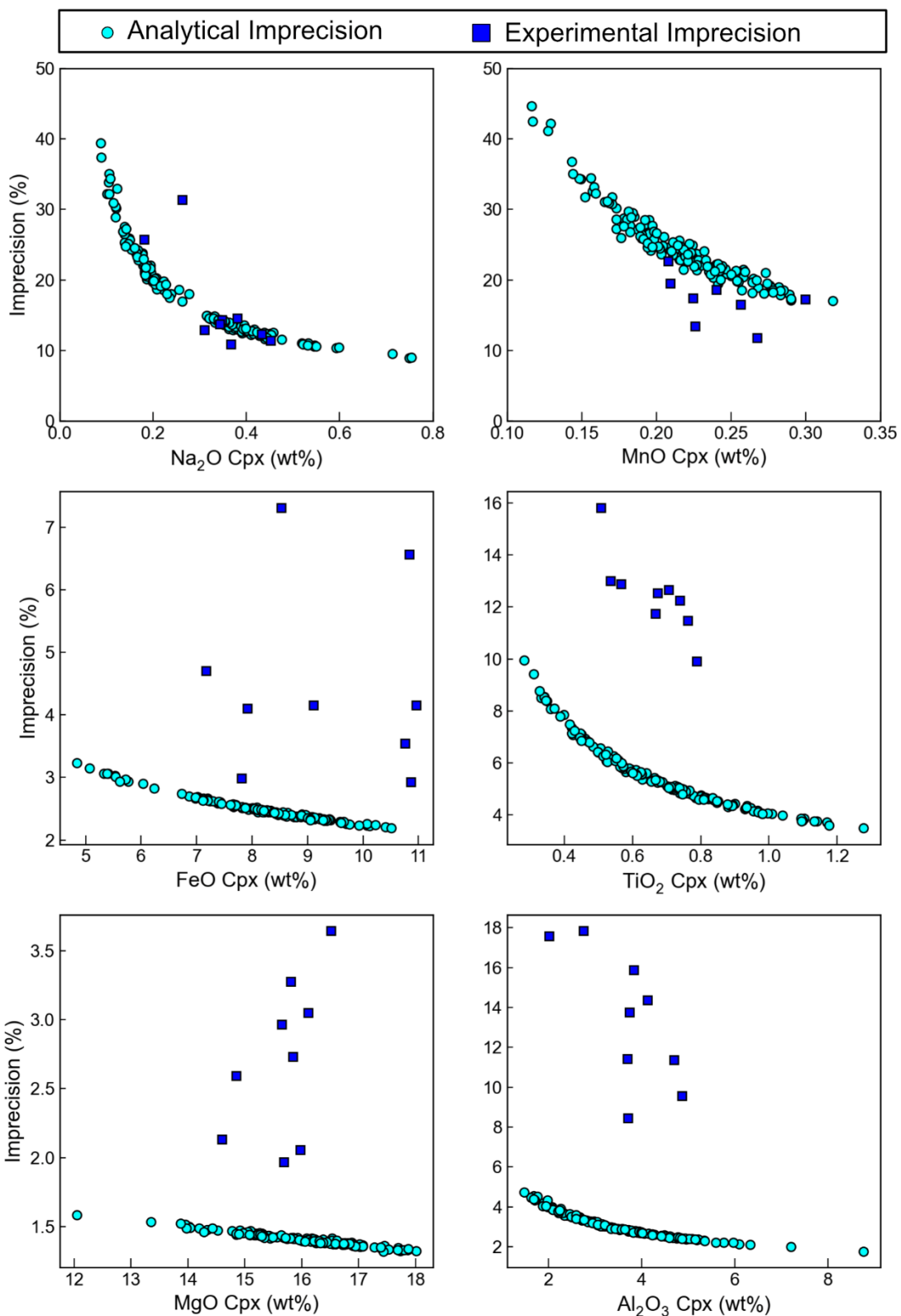
Supporting Figure 14 – Correlations between elements in Exp. BM40 from Melekhova et al. (2015)



Supporting Figure 15 – Correlations between elements in Exp. CE-7 from Erdmann et al. (2016).

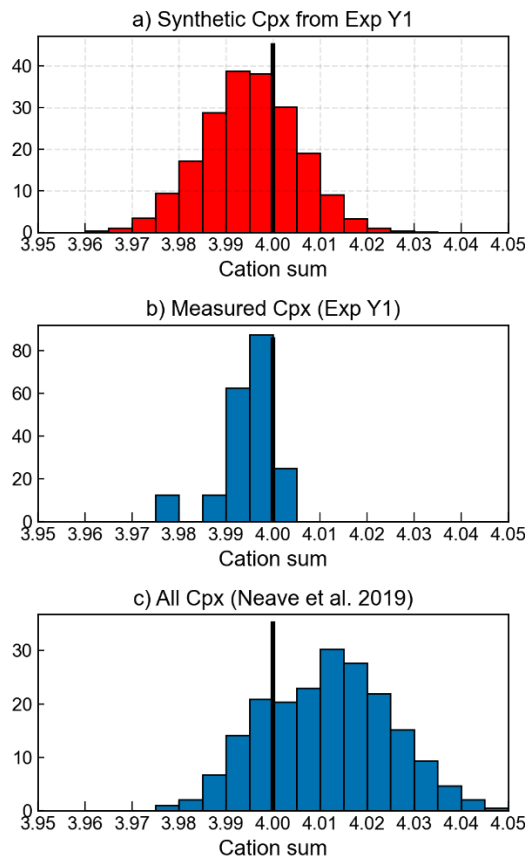


Supporting Fig. 16 – Figures comparing analytical imprecision (orange and red dots) to the variability observed in each experiment of Krawczynski et al. (2012- yellow squares).

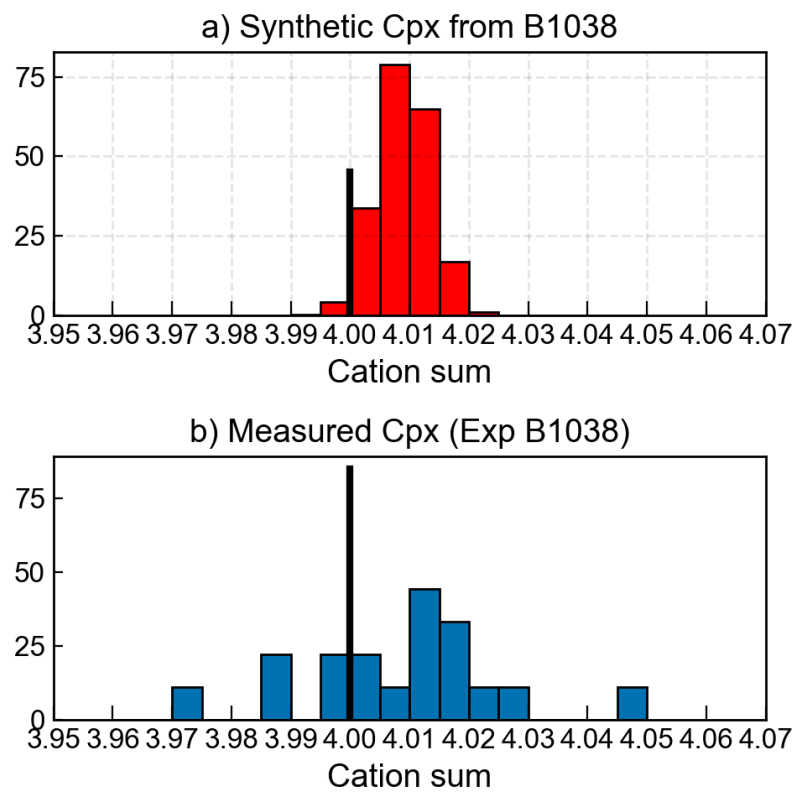


Supporting Fig. 17 - Figures comparing analytical imprecision (cyan dots) to the variability observed in each experiment of Neave et al. (2019; blue squares).

4. Additional Information regarding Monte Carlo Simulations



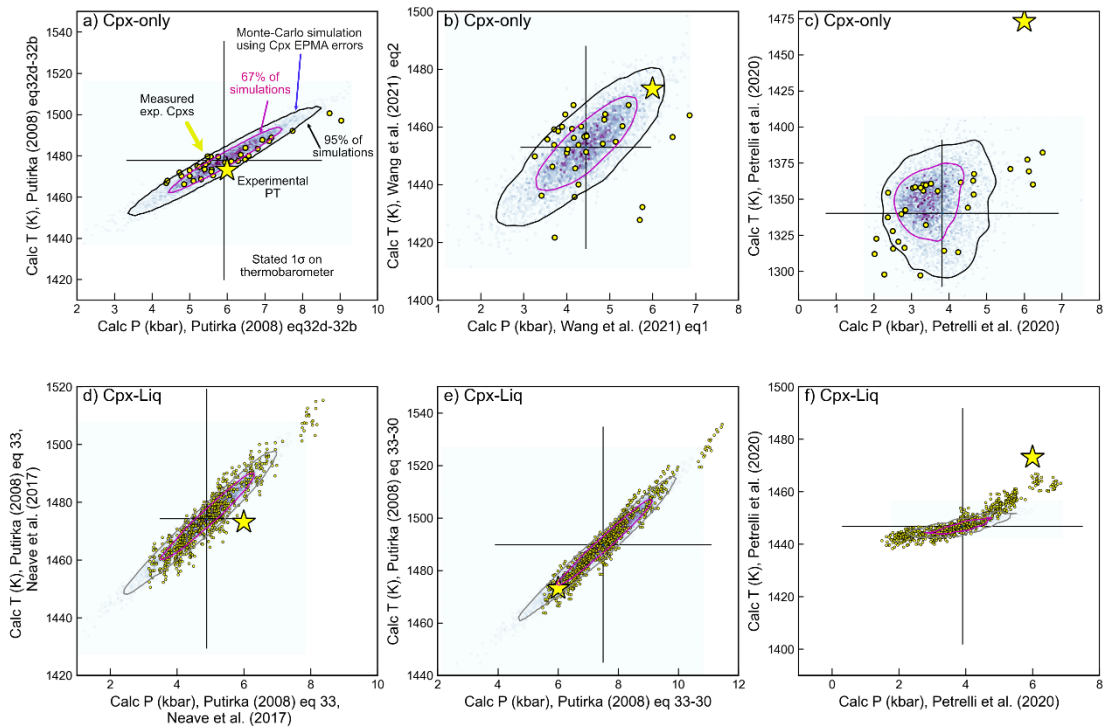
Supporting Fig. 18 – Distribution of cation sums in synthetic Cpx (part a) vs measured Cpx in that experiment, and measured Cpx in all experiments of Neave et al. (2019). Y axis shows probability density.



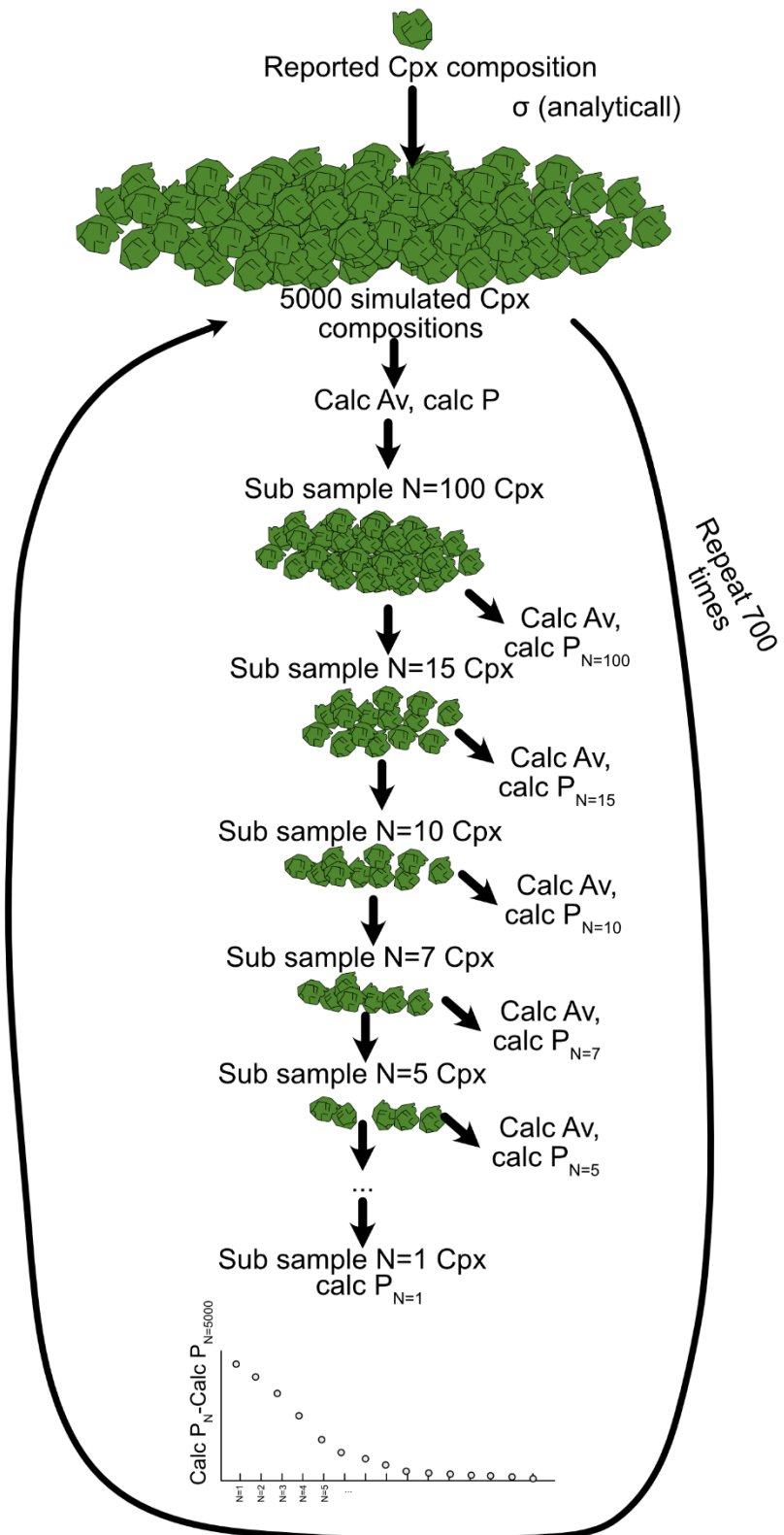
Supporting Fig. 19 – Cation sums for simulated Cpx from Krawczynski et al. (2012) compared to those in the experiment we are trying to simulate.



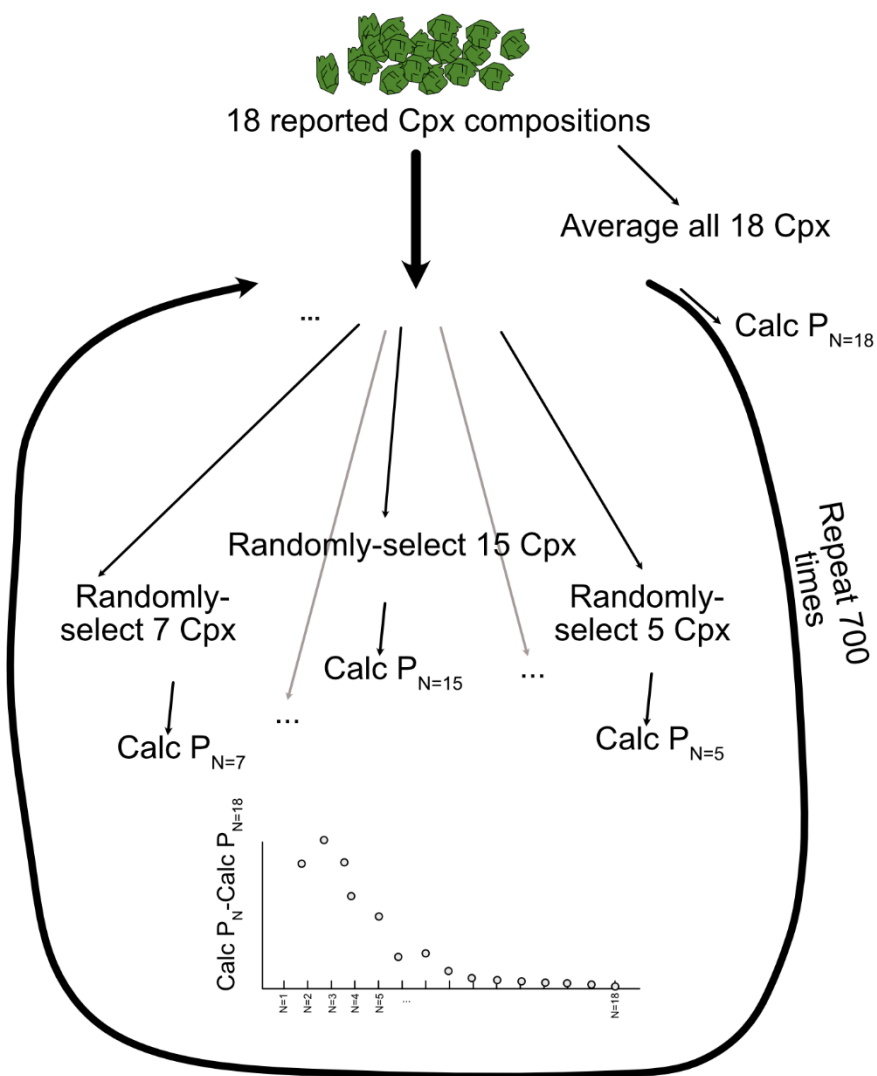
B1084-10 - 6 kbar, 1200 °C, Au-Pd, 48 hrs



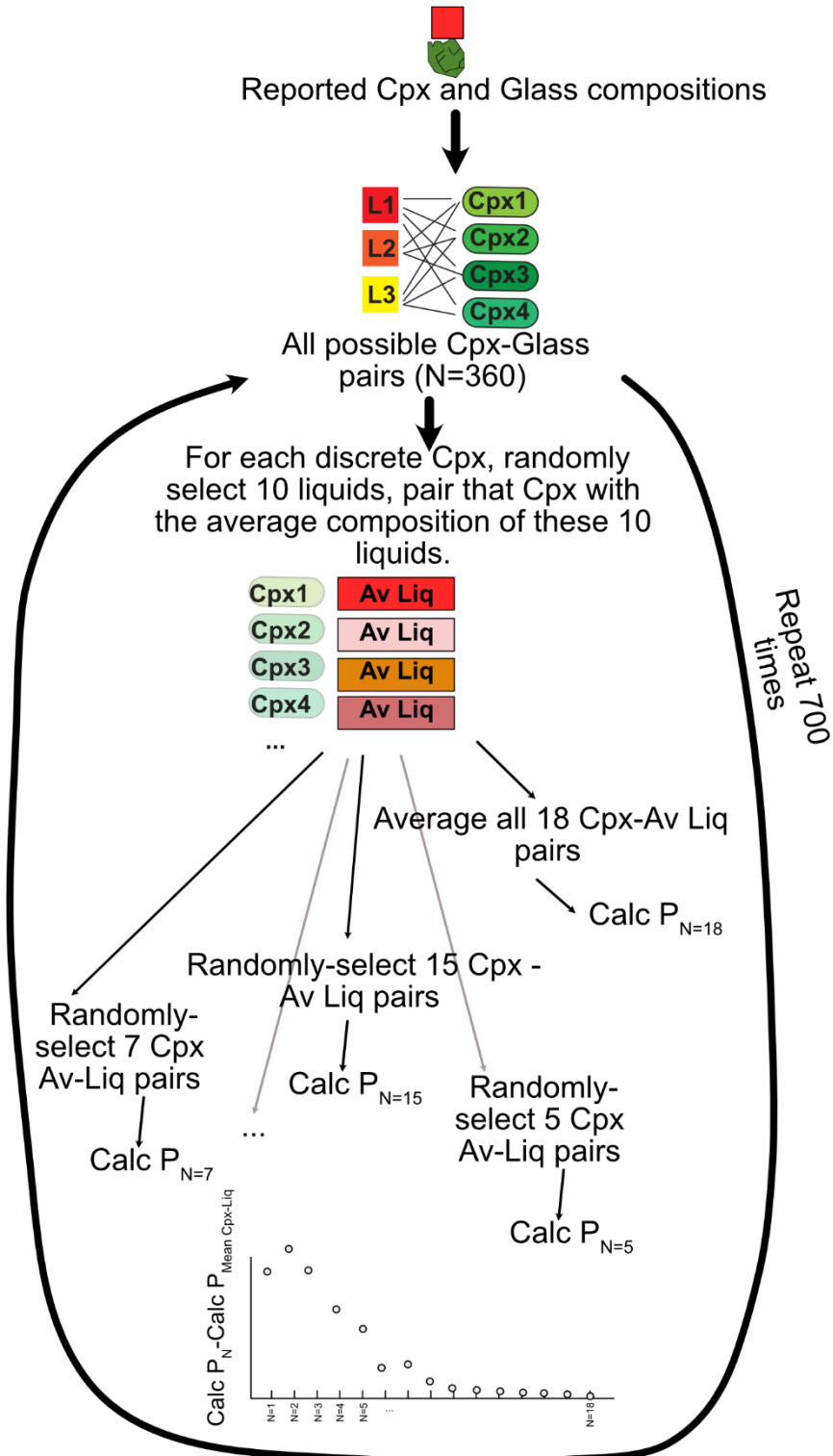
Supporting Figure 20 – As for Fig. 8 in the main text, but showing experiment B1084-10 from Neave et al. (2019).



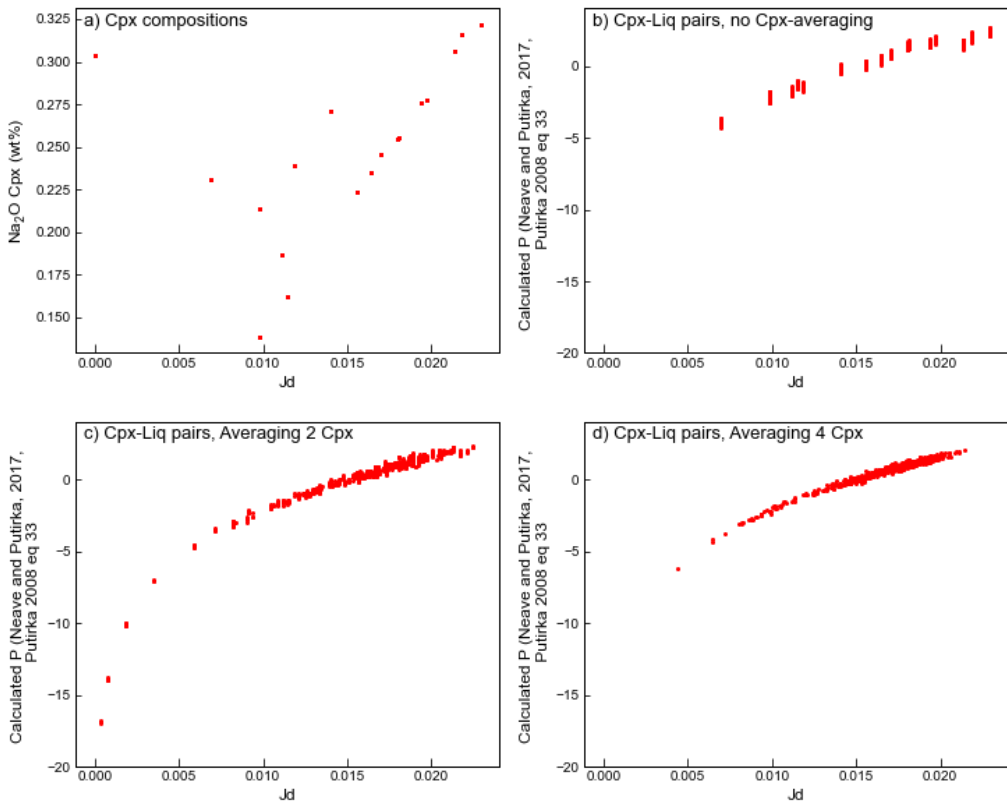
Supporting Fig. 21 – Schematic of the for-loop used to calculate the discrepancy in pressure as a function of the number of Cpx averaged for the Neave et al. (2017) experiment shown in Fig. 10a-b.



Supporting Fig 22— Schematic of the for loop used for subsampling the Cpx of Krawczynski et al. (2012) in Fig 10 c-d of the main text.



Supporting Fig 23— Schematic of the for loop used for subsampling the Cpx-Liq experiments of Krawczynski et al. (2012) in Fig 10 e-f of the main text.

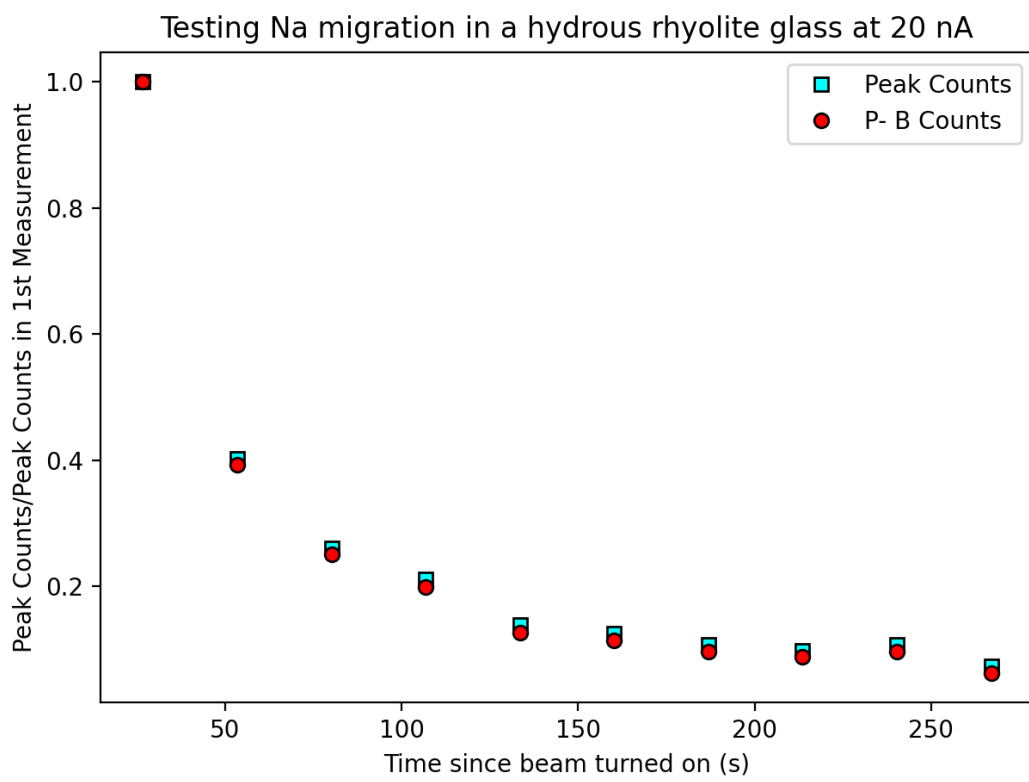


Supporting Fig. 24 –a) Cpx compositions from Experiment B1038 of Krawczynski et al. (2012). b) calculated Cpx-Liq pressures vs. Jd for measured Cpx matched with various liquid compositions. c-d) Cpx-Liq pressures averaging 2 and 4 Cpx. In c), a number of Cpx have very low, but non-zero Jd contents, resulting in strongly negative calculated pressures.

5. Investigating Na Migration in Pyroxene during EPMA analyses.

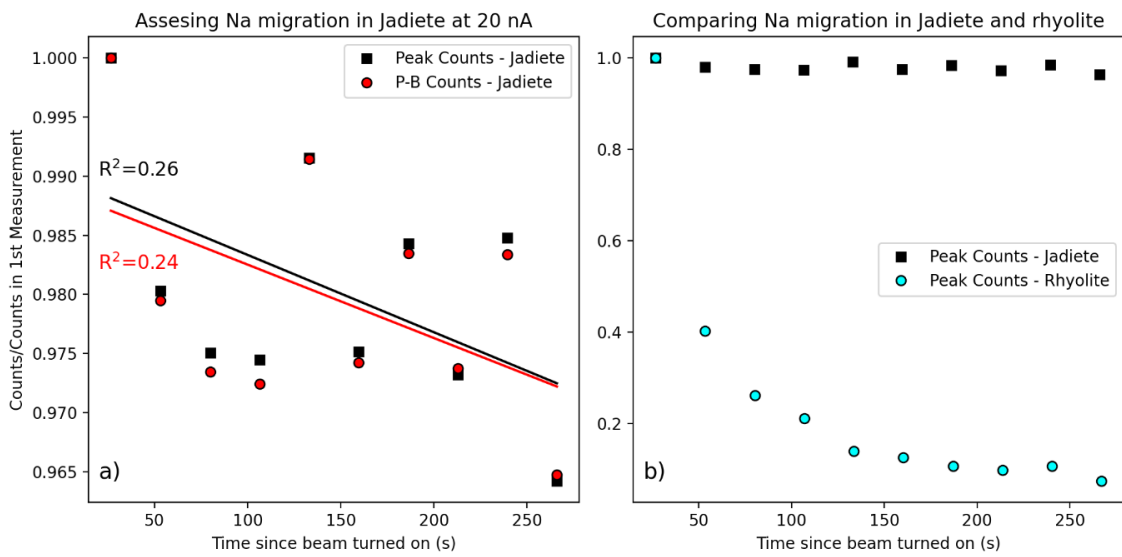
Analyses were performed on the SX100 at Oregon State at 15 kV with a beam size of 1 μm , using beam currents of 20, 40 and 100 nA. Na was analysed on the LTAP crystal, using Labradorite as a primary calibration standard (calibration performed at 20 nA).

We use three separate methods to track whether Na is migrating under the electron beam. First, we use the P-B-P-B “Subcounting” routine in the PeakSight software. The software splits the acquisition time of any given elements into 10 windows. Then, it measures the Peak counts, Background1 counts, Background 2 counts for each the first measurement. It then cycles through this for as many N as are specified. To validate this method, we first track the change in Na counts within a hydrous rhyolitic glass (3 wt% H₂O), which should show extensive migration. We plot the change in peak counts relative to the first measurement. Peak and P-B counts decline rapidly, to values only 0.4X the original after 50s of beam exposure, with a tail off to very low Na counts after 100s (Supporting Fig. 22).

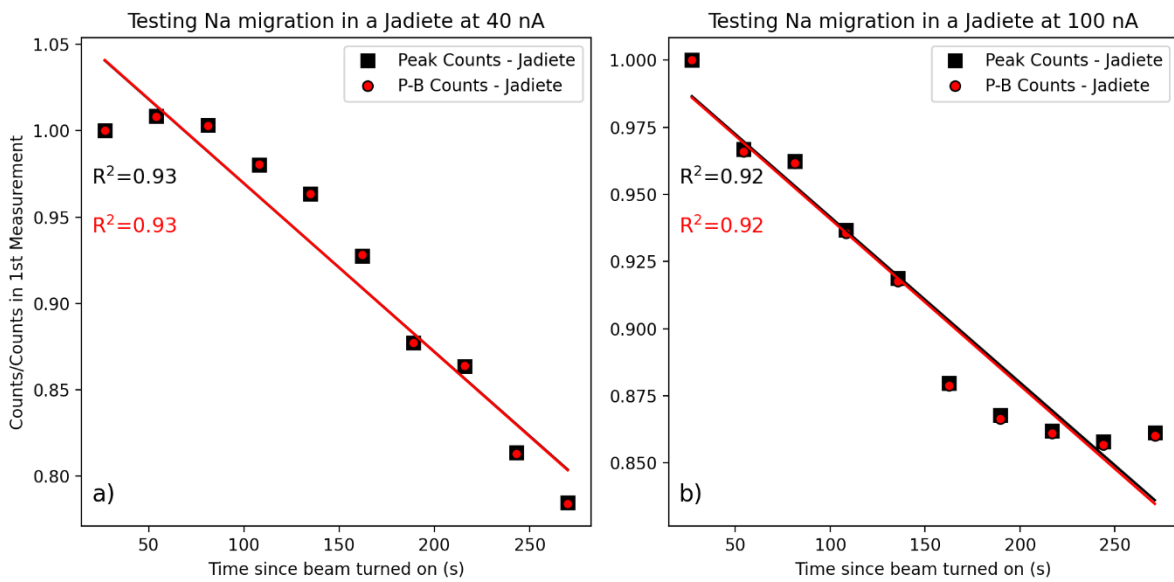


Supporting Figure 25 – Tracking Na counts in a hydrous rhyolite glass using the sub-counting P-B-P routine at 20 nA over >250 s.

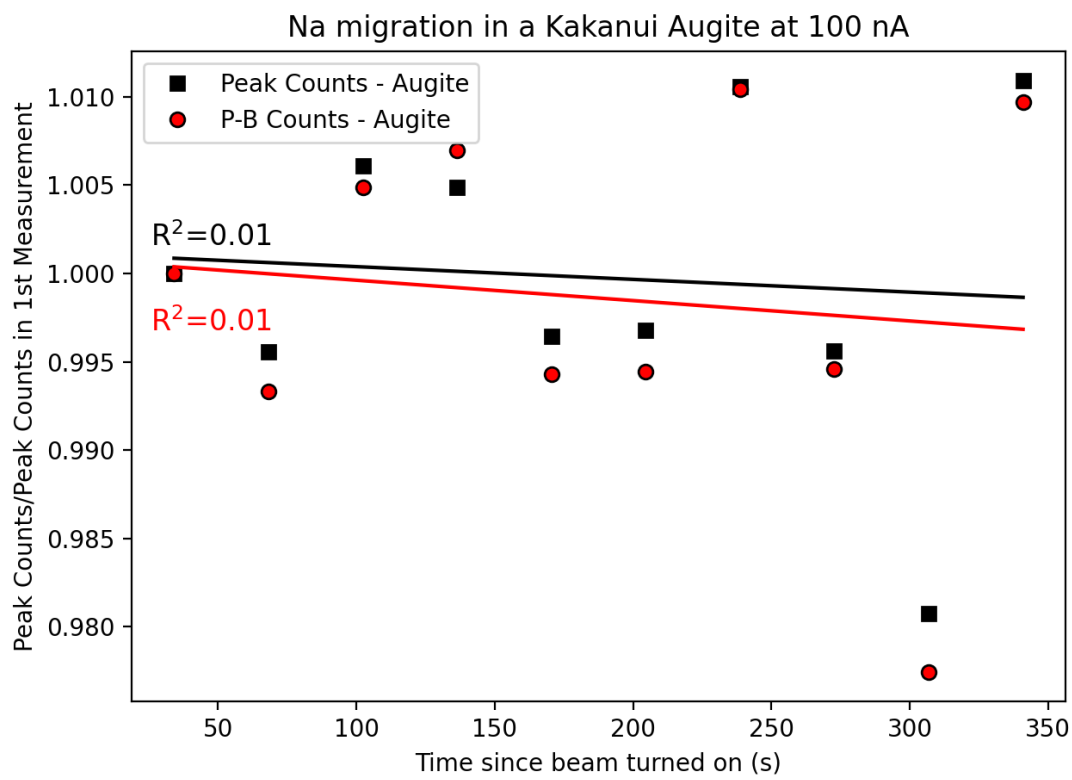
In contrast, when we perform the same P-B-P routine on a Jadeite standard, counts only decline by ~4% over 250 s at 20 nA (Supporting Figure 23a), with a small r^2 value (compare to rhyolite in Supporting Figure 23b). At higher currents (40 and 100 nA) counts decline by 15–20% over 250 s (Supporting Figure 24). In contrast, even at 100 nA, Na Peak counts, and Peak-Background counts show no noticeable change with time in natural augite (Kakanui Augite, 1.1 wt% Na, Supporting Figure 25). These subcounting routines demonstrate that while glasses are highly beam sensitive and undergone substantial beam loss, Jadeite is only very slightly beam sensitive at 20 nA over prolonged count periods, and only shows strong correlations between peak counts and time at 40 nA and 100 nA. In contrast, even for prolonged count times (>250s) and very high probe currents (100 nA), natural pyroxenes undergo no noticeable migration of Na.



Supporting Figure 26 – a) Tracking peak and peak – background (P-B) counts in Jadeite vs. time at 20 nA. b) The changes are entirely overwhelmed by those seen in rhyolites.

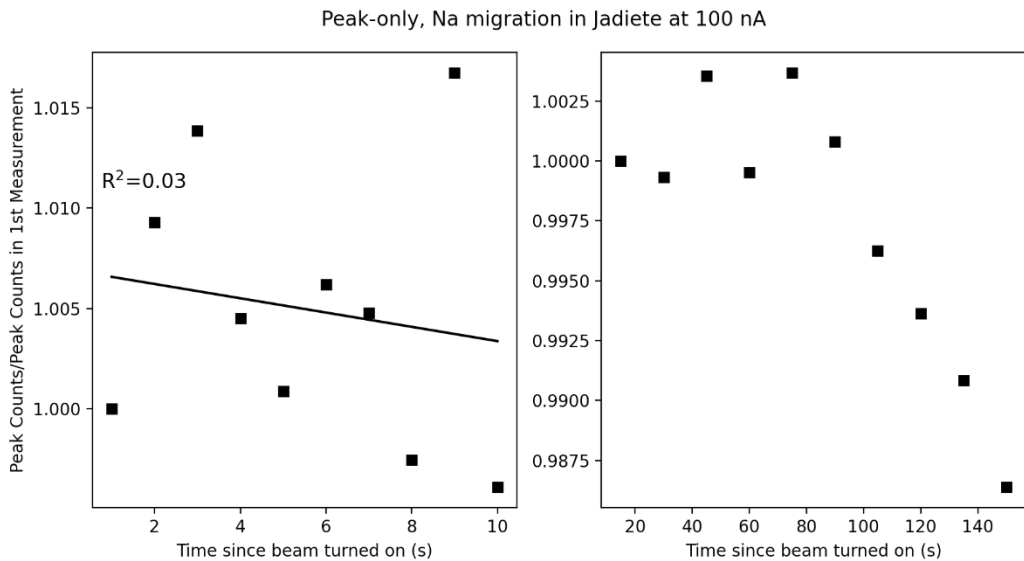


Supporting Figure 27 – Tracking peak and peak – background (P-B) counts in Jadeite vs. time at 40 nA (a) and 100 nA (b).



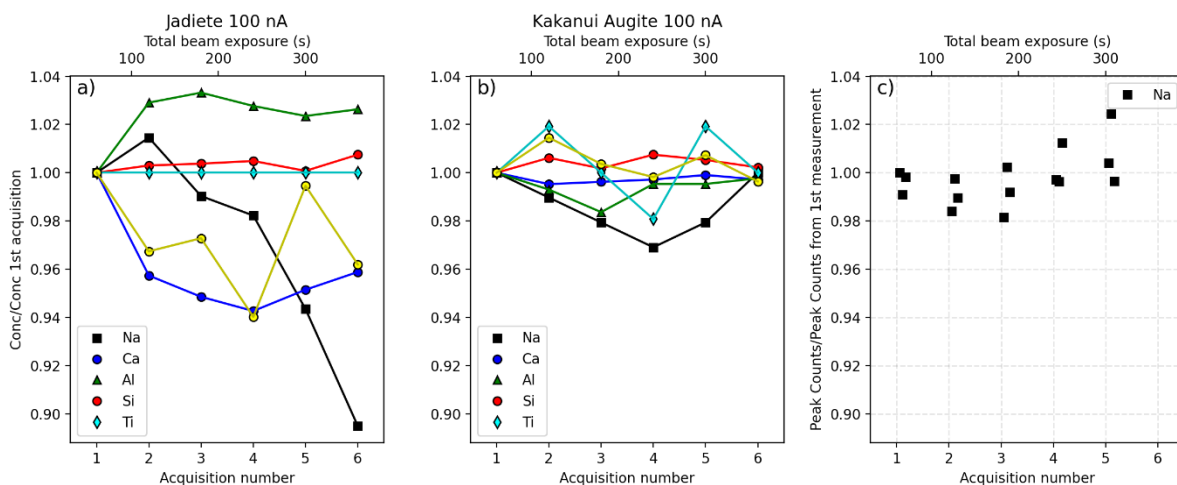
Supporting Figure 28 – Tracking changes in Na counts with time in Kakanui Augite at 100 nA.

Beam sensitivity of Jadeite is important in that it is often used as a primary calibration standard for Na in pyroxene. Given that P-B-P routines are missing gaps in time as the spectrometer position is constantly being adjusted, we also perform a routine where the Na peak is measured in short increments, without measuring backgrounds (as Supporting Figs. 22-25 show that Peak-counts and P-B counts show very similar trends). First, we count on the peak ten times for 1-second intervals and then count on the peak ten times over 15 s intervals (Supporting Figure 26). These graphs demonstrates that, even at 100 nA, Jadeite only begins to lose Na after 80s of beam exposure. This indicates that at common calibration conditions (e.g., 20-40 nA, 10-30s), Na migration in Jadeite is not a major problem.



Supporting Figure 29 – Tracking Peak counts on Na over 10s and 150s (in 10 discrete measurement intervals).

We perform one additional set of tests at 100 nA to investigate changes in elemental concentrations where we perform a relatively short (1 minute total beam exposure) analytical routine for Na-Ca-Al-Si-Ti on a single point on Jadeite, and obtain a quantitative analysis for this point (in terms of wt%, Supporting Figure 27a). We then perform a repeat analysis without moving the stage. We compare element concentrations from 6 repeated measurements to those measured in the first spot. For Jadeite, the only element showing noticeable unidirectional changes is Na, declining by ~10 % relative after 6 minutes of beam exposure. For Kakanui augite, we use the same routine, but also split each measurement of the Na peak into 3 P-P-P subcount routines (3 seconds each), and apply the zero-time-intersection correction in the software. None of the 6 acquisitions show any coherent trends between Na counts and time (Supporting Figure 27c) so very similar results would have been achieved without using a zero time intercept.



Supporting Figure 30 – a) Tracking changes in elemental concentrations during 6 repeated analyses (60s of beam exposure each) in the same stage position on Jadeite, with no zero-time-intercept correction. b) Same for Kakanui augite, but using a zero-time-intercept correction for Na

based on 3 subcounts on the Na Peak during each acquisition. In c), the counts for these are shown. There are no coherent changes with time above the noise of the measurement.

Additional References

- Akella, J., 1976. Garnet pyroxene equilibria in the system CaSiOrMgSiOs-AlrOe and in a natural mineral mixture. *American Mineralogist*, V61, pp 589-598
- Almeev, R.R., Holtz, F., Ariskin, A.A., Kimura, J.-I., 2013. Storage conditions of Bezymianny Volcano parental magmas: results of phase equilibria experiments at 100 and 700 MPa. *Contrib Mineral Petrol* 166, 1389–1414. <https://doi.org/10.1007/s00410-013-0934-x>
- Alonso-Perez, R., Müntener, O., Ulmer, P., 2009. Igneous garnet and amphibole fractionation in the roots of island arcs: experimental constraints on andesitic liquids. *Contrib Mineral Petrol* 157, 541–558. <https://doi.org/10.1007/s00410-008-0351-8>
- Andújar, J., Scaillet, B., Pichavant, M., Druitt, T.H., 2015. Differentiation Conditions of a Basaltic Magma from Santorini, and its Bearing on the Production of Andesite in Arc Settings. *Journal of Petrology* 56, 765–794. <https://doi.org/10.1093/petrology/egv016>
- Baker, D.R., Eggler, D.H., 1987. Compositions of anhydrous and hydrous melts coexisting with plagioclase, augite, and olivine or low-Ca pyroxene from 1 atm to 8 kbar: Application to the Aleutian volcanic center of Atka. *American Mineralogist* 72.
- Baker, M.B., Grove, T.L., Price, R., 1994. Primitive basalts and andesites from the Mt. Shasta region, N. California: products of varying melt fraction and water content. *Contr. Mineral. and Petrol.* 118, 111–129. <https://doi.org/10.1007/BF01052863>
- Barclay, J., 2004. A Hornblende Basalt from Western Mexico: Water-saturated Phase Relations Constrain a Pressure-Temperature Window of Eruptibility. *Journal of Petrology* 45, 485–506. <https://doi.org/10.1093/petrology/egg091>
- Berndt, J., 2004. An Experimental Investigation of the Influence of Water and Oxygen Fugacity on Differentiation of MORB at 200 MPa. *Journal of Petrology* 46, 135–167. <https://doi.org/10.1093/petrology/egh066>
- Berndt, J., Holtz, F., Koepke, J., 2001. Experimental constraints on storage conditions in the chemically zoned phonolitic magma chamber of the Laacher See volcano. *Contrib Mineral Petrol* 140, 469–486. <https://doi.org/10.1007/PL00007674>
- Blatter, D.L., Carmichael, I.S.E., 2001. Hydrous phase equilibria of a Mexican high-silica andesite: A candidate for a mantle origin? *Geochimica et Cosmochimica Acta* 65, 4043–4065. [https://doi.org/10.1016/S0016-7037\(01\)00708-6](https://doi.org/10.1016/S0016-7037(01)00708-6)

Blatter, D.L., Sisson, T.W., Hankins, W.B., 2013. Crystallization of oxidized, moderately hydrous arc basalt at mid- to lower-crustal pressures: implications for andesite genesis. *Contrib Mineral Petrol* 166, 861–886. <https://doi.org/10.1007/s00410-013-0920-3>

Blundy, J.D., Robinson, J.A.C., Wood, B.J., 1998. Heavy REE are compatible in clinopyroxene on the spinel Iherzolite solidus. *Earth and Planetary Science Letters* 160, 493–504. [https://doi.org/10.1016/S0012-821X\(98\)00106-X](https://doi.org/10.1016/S0012-821X(98)00106-X)

Cadoux, A., Scaillet, B., Druitt, T.H., Deloule, E., 2014. Magma Storage Conditions of Large Plinian Eruptions of Santorini Volcano (Greece). *Journal of Petrology* 55, 1129–1171. <https://doi.org/10.1093/petrology/egu021>

Carroll, M.R., Wyllie, P.J., 1989. Experimental Phase Relations in the System Tonalite-Peridotite-H₂O at 15 kb; Implications for Assimilation and Differentiation Processes near the Crust-Mantle Boundary. *Journal of Petrology* 30, 1351–1382. <https://doi.org/10.1093/petrology/30.6.1351>

Costa, F., 2004. Petrological and Experimental Constraints on the Pre-eruption Conditions of Holocene Dacite from Volcan San Pedro (36 S, Chilean Andes) and the Importance of Sulphur in Silicic Subduction-related Magmas. *Journal of Petrology* 45, 855–881. <https://doi.org/10.1093/petrology/egg114>

Di Carlo, I., 2006. Experimental Crystallization of a High-K Arc Basalt: the Golden Pumice, Stromboli Volcano (Italy). *Journal of Petrology* 47, 1317–1343. <https://doi.org/10.1093/petrology/egl011>

Draper, D.S., Green, T.H., 1999. P-T phase relations of silicic, alkaline, aluminous liquids: new results and applications to mantle melting and metasomatism. *Earth and Planetary Science Letters* 170, 255–268. [https://doi.org/10.1016/S0012-821X\(99\)00111-9](https://doi.org/10.1016/S0012-821X(99)00111-9)

Draper, D.S., Johnston, A.D., 1992. Anhydrous PT phase relations of an Aleutian high-MgO basalt: an investigation of the role of olivine-liquid reaction in the generation of arc high-alumina basalts. *Contr. Mineral. and Petrol.* 112, 501–519. <https://doi.org/10.1007/BF00310781>

Erdmann, S., Martel, C., Pichavant, M., Bourdier, J.-L., Champallier, R., Komorowski, J.-C., Cholik, N., 2016. Constraints from Phase Equilibrium Experiments on Pre-eruptive Storage Conditions in Mixed Magma Systems: a Case Study on Crystal-rich Basaltic Andesites from Mount Merapi, Indonesia. *J. Petrology* 57, 535–560. <https://doi.org/10.1093/petrology/egw019>

Feig, S.T., Koepke, J., Snow, J.E., 2010. Effect of oxygen fugacity and water on phase equilibria of a hydrous tholeiitic basalt. *Contrib Mineral Petrol* 160, 551–568. <https://doi.org/10.1007/s00410-010-0493-3>

Feig, S.T., Koepke, J., Snow, J.E., 2006. Effect of water on tholeiitic basalt phase equilibria: an experimental study under oxidizing conditions. *Contrib Mineral Petrol* 152, 611–638. <https://doi.org/10.1007/s00410-006-0123-2>

Firth, C., Adam, J., Turner, S., Rushmer, T., Brens, R., Green, T.H., Erdmann, S., O'Neill, H., 2019. Experimental constraints on the differentiation of low-alkali magmas beneath the Tonga arc: Implications for the origin of arc tholeiites. *Lithos* 344–345, 440–451. <https://doi.org/10.1016/j.lithos.2019.07.008>

Fram, M., Longhi, John, 1992. Phase equilibria of dikes associated with Proterozoic anorthosite complexes. *American Mineralogist*.v77, 605-616

Gee, L.L., Sack, R.O., 1988. Experimental Petrology of Melilite Nephelinites. *Journal of Petrology* 29, 1233–1255. <https://doi.org/10.1093/petrology/29.6.1233>

Hamada, M., Fujii, T., 2008. Experimental constraints on the effects of pressure and H₂O on the fractional crystallization of high-Mg island arc basalt. *Contrib Mineral Petrol* 155, 767–790. <https://doi.org/10.1007/s00410-007-0269-6>

Husen, A., Almeev, R.R., Holtz, F., 2016. The Effect of H₂O and Pressure on Multiple Saturation and Liquid Lines of Descent in Basalt from the Shatsky Rise. *Journal of Petrology* 57, 309–344. <https://doi.org/10.1093/petrology/egw008>

Kawamoto, T., 1996. Experimental constraints on differentiation and H₂O abundance of calc-alkaline magmas. *Earth and Planetary Science Letters* 144, 577–589. [https://doi.org/10.1016/S0012-821X\(96\)00182-3](https://doi.org/10.1016/S0012-821X(96)00182-3)

Kennedy, A.K., Grove, T.L., Johnson, R.W., 1990. Experimental and major element constraints on the evolution of lavas from Lihir Island, Papua New Guinea. *Contr. Mineral. and Petrol.* 104, 722–734. <https://doi.org/10.1007/BF01167289>

Koepke, J., Botcharnikov, R.E., Natland, J.H., 2018. Crystallization of late-stage MORB under varying water activities and redox conditions: Implications for the formation of highly evolved lavas and oxide gabbro in the ocean crust. *Lithos* 323, 58–77. <https://doi.org/10.1016/j.lithos.2018.10.001>

Krawczynski, M.J., Grove, T.L., Behrens, H., 2012. Amphibole stability in primitive arc magmas: effects of temperature, H₂O content, and oxygen fugacity. *Contrib Mineral Petrol* 164, 317–339. <https://doi.org/10.1007/s00410-012-0740-x>

Laporte, D., Toplis, M.J., Seyler, M., Devidal, J.-L., 2004. A new experimental technique for extracting liquids from peridotite at very low degrees of melting: application to partial melting of depleted peridotite. *Contributions to Mineralogy and Petrology* 146, 463–484. <https://doi.org/10.1007/s00410-003-0509-3>

Maaløe, S., 2004. The PT-phase relations of an MgO-rich Hawaiian tholeiite: the compositions of primary Hawaiian tholeiites. *Contrib Mineral Petrol* 148, 236–246. <https://doi.org/10.1007/s00410-004-0601-3>

Mandler, B.E., Donnelly-Nolan, J.M., Grove, T.L., 2014. Straddling the tholeiitic/calc-alkaline transition: the effects of modest amounts of water on magmatic differentiation at Newberry Volcano, Oregon. *Contrib Mineral Petrol* 168, 1066. <https://doi.org/10.1007/s00410-014-1066-7>

McCoy, T.J., Lofgren, G.E., 1999. Crystallization of the Zagami shergottite: an experimental study. *Earth and Planetary Science Letters* 173, 397–411. [https://doi.org/10.1016/S0012-821X\(99\)00241-1](https://doi.org/10.1016/S0012-821X(99)00241-1)

Melekhova, E., Blundy, J., Robertson, R., Humphreys, M.C.S., 2015. Experimental Evidence for Polybaric Differentiation of Primitive Arc Basalt beneath St. Vincent, Lesser Antilles. *Journal of Petrology* 56, 161–192. <https://doi.org/10.1093/petrology/egu074>

Métrich, N., Rutherford, M.J., 1998. Low Pressure Crystallization Paths of H₂O-Saturated Basaltic-Hawaiitic Melts from Mt Etna: Implications for Open-System Degassing of Basaltic Volcanoes. *Geochimica et Cosmochimica Acta* 62, 1195–1205. [https://doi.org/10.1016/S0016-7037\(98\)00048-9](https://doi.org/10.1016/S0016-7037(98)00048-9)

Minitti, M.E., Rutherford, M.J., 2000. Genesis of the Mars Pathfinder ?sulfur-free? rock from SNC parental liquids. *Geochimica et Cosmochimica Acta* 64, 2535–2547. [https://doi.org/10.1016/S0016-7037\(00\)00366-5](https://doi.org/10.1016/S0016-7037(00)00366-5)

Nandedkar, R.H., Ulmer, P., Müntener, O., 2014. Fractional crystallization of primitive, hydrous arc magmas: an experimental study at 0.7 GPa. *Contrib Mineral Petrol* 167, 1015. <https://doi.org/10.1007/s00410-014-1015-5>

Neave, D.A., Bali, E., Guðfinnsson, G.H., Halldórsson, S.A., Kahl, M., Schmidt, A.-S., Holtz, F., 2019. Clinopyroxene–Liquid Equilibria and Geothermobarometry in Natural and Experimental Tholeiites: the 2014–2015 Holuhraun Eruption, Iceland. *Journal of Petrology* 60, 1653–1680. <https://doi.org/10.1093/petrology/egz042>

Nielsen, R.L., Gallahan, W.E., Newberger, F., 1992. Experimentally determined mineral-melt partition coefficients for Sc, Y and REE for olivine, orthopyroxene, pigeonite, magnetite and ilmenite. *Contrib Mineral Petrol* 110, 488–499. <https://doi.org/10.1007/BF00344083>

Parat, F., Streck, M., Holtz, F., Almeev, R.R., 2014. Experimental study into the petrogenesis of crystal-rich basaltic to andesitic magmas at Arenal volcano. *Contributions to Mineralogy and Petrology*, v168. <https://doi.org/10.1007/s00410-014-1040-4>

Pertermann, M., 2003. Anhydrous Partial Melting Experiments on MORB-like Eclogite: Phase Relations, Phase Compositions and Mineral-Melt Partitioning of Major Elements at 2-3 GPa. *Journal of Petrology* 44, 2173–2201. <https://doi.org/10.1093/petrology/egg074>

Pertermann, M., Lundstrom, C.C., 2006. Phase equilibrium experiments at 0.5 GPa and 1100–1300 °C on a basaltic andesite from Arenal volcano, Costa Rica. *Journal of Volcanology and Geothermal Research* 157, 222–235. <https://doi.org/10.1016/j.jvolgeores.2006.03.043>

Pichavant, M., Macdonald, R., 2007. Crystallization of primitive basaltic magmas at crustal pressures and genesis of the calc-alkaline igneous suite: experimental evidence from St Vincent, Lesser Antilles arc. *Contrib Mineral Petrol* 154, 535–558. <https://doi.org/10.1007/s00410-007-0208-6>

Prouteau, G., 2003. Experimental Constraints on the Origin of the 1991 Pinatubo Dacite. *Journal of Petrology* 44, 2203–2241. <https://doi.org/10.1093/petrology/egg075>

Rader, E.L., Larsen, J.F., 2013. Experimental phase relations of a low MgO Aleutian basaltic andesite at $\text{XH}_2\text{O} = 0.7\text{--}1$. *Contrib Mineral Petrol* 166, 1593–1611. <https://doi.org/10.1007/s00410-013-0944-8>

Rushmer, T., 1993. Experimental high-pressure granulites: Some applications to natural mafic xenolith suites and Archean granulite terranes. *Geol* 21, 411. [https://doi.org/10.1130/0091-7613\(1993\)021<0411:EHPGSA>2.3.CO;2](https://doi.org/10.1130/0091-7613(1993)021<0411:EHPGSA>2.3.CO;2)

Scaillet, B., 2003. Experimental Constraints on the Relationships between Peralkaline Rhyolites of the Kenya Rift Valley. *Journal of Petrology* 44, 1867–1894.
<https://doi.org/10.1093/petrology/egg062>

Scoates, J.S., Lo Cascio, M., Weis, D., Lindsley, D.H., 2006. Experimental constraints on the origin and evolution of mildly alkalic basalts from the Kerguelen Archipelago, Southeast Indian Ocean. *Contrib Mineral Petrol* 151, 582–599. <https://doi.org/10.1007/s00410-006-0070-y>

Springer, W., Seck, H.A., 1997. Partial fusion of basic granulites at 5 to 15 kbar: implications for the origin of TTG magmas. *Contributions to Mineralogy and Petrology* 127, 30–45.
<https://doi.org/10.1007/s004100050263>

Toplis, M.J., Corgne, A., 2002. An experimental study of element partitioning between magnetite, clinopyroxene and iron-bearing silicate liquids with particular emphasis on vanadium. *Contrib Mineral Petrol* 144, 22–37. <https://doi.org/10.1007/s00410-002-0382-5>

Tsuruta, K., Takahashi, E., 1998. Melting study of an alkali basalt JB-1 up to 12.5 GPa: behavior of potassium in the deep mantle. *Physics of the Earth and Planetary Interiors* 107, 119–130. [https://doi.org/10.1016/S0031-9201\(97\)00130-1](https://doi.org/10.1016/S0031-9201(97)00130-1)

Ubide, T., Mollo, S., Zhao, J., Nazzari, M., Scarlato, P., 2019. Sector-zoned clinopyroxene as a recorder of magma history, eruption triggers, and ascent rates. *Geochimica et Cosmochimica Acta* 251, 265–283. <https://doi.org/10.1016/j.gca.2019.02.021>

Ulmer, P., Kaegi, R., Müntener, O., 2018. Experimentally Derived Intermediate to Silica-rich Arc Magmas by Fractional and Equilibrium Crystallization at 1·0 GPa: an Evaluation of Phase Relationships, Compositions, Liquid Lines of Descent and Oxygen Fugacity. *Journal of Petrology* 59, 11–58. <https://doi.org/10.1093/petrology/egy017>

Wang, W., Takahashi, E., 1999. Subsolidus and melting experiments of a K-rich basaltic composition to 27 GPa; implication for the behavior of potassium in the mantle. *American Mineralogist* 84, 357–361. <https://doi.org/10.2138/am-1999-0319>

Wasylenki, L.E., 2003. Near-solidus Melting of the Shallow Upper Mantle: Partial Melting Experiments on Depleted Peridotite. *Journal of Petrology* 44, 1163–1191. <https://doi.org/10.1093/petrology/44.7.1163>

Waters, L.E., Cottrell, E., Coombs, M.L., Kelley, K.A., 2021. Generation of Calc-Alkaline Magmas during Crystallization at High Oxygen Fugacity: An Experimental and Petrologic Study of Tephrae from Buldir Volcano, Western Aleutian Arc, Alaska, USA. *Journal of Petrology* 62, egaa104. <https://doi.org/10.1093/petrology/egaa104>

Wood, B.J., Trigila, R., 2001. Experimental determination of aluminous clinopyroxene–melt partition coefficients for potassic liquids, with application to the evolution of the Roman province potassic magmas. *Chemical Geology* 172, 213–223. [https://doi.org/10.1016/S0009-2541\(00\)00259-X](https://doi.org/10.1016/S0009-2541(00)00259-X)